Nat. Hazards Earth Syst. Sci., 26, 6093–6115, 2026
https://doi.org/10.5194/nhess-26-6093-2026
© Author(s) 2026. This work is distributed under
the Creative Commons Attribution 4.0 License.

Natural Hazards and Earth System Sciences
Open Access
EGU

National-scale debris-flow hazard indication modelling for Swiss railway infrastructure

Feiko Bernard van Zadelhoff[1,2], **Yves Bühler**[1,2], **and Michael Bründl**[1,2]

[1]WSL Institute for Snow and Avalanche Research SLF, Davos, Switzerland
[2]Climate Change, Extremes and Natural Hazards in Alpine Regions Research Centre CERC, Davos, Switzerland

Correspondence: Feiko Bernard van Zadelhoff (feiko.vanzadelhoff@slf.ch)

Received: 30 July 2026 – Discussion started: 19 August 2026
Revised: 8 October 2026 – Accepted: 9 November 2026 – Published: 25 November 2026

Abstract. Debris flows are among the most destructive alpine hazards, threatening settlements and critical infrastructure with average annual damages in Switzerland of CHF 321 million. Hazard indication modelling of debris flows, among other hazards, offers the possibility to identify hazard hot spots at a regional and national scale. Additionally it lays the foundation for future scenario modelling. We present the Large-Scale Hazard Indication Modelling (LSHIM) framework for debris flows as commissioned by the Swiss federal railway (SBB) with guiding value return periods of 30, 100, and 300 years. For susceptibility modelling, we combine high-resolution digital terrain models, climatic and geologic layers, and statistical modelling with a random forest approach. Susceptibility is cross-validated against the Swiss event database (StorMe) with an average accuracy of 81.4 % and application results in 16 756 possible release areas. Dynamic runout is calculated with a tailored version of RAMMS::Debrisflow, where we define hydrograph volume from MeteoSchweiz-modelled extreme precipitation. Landscape erosivity is assessed by geology and geomorphology. Results indicate 55, 76, and 85 km of railway affected by debris flow hazard for a 30-, 100-, and 300-year return period, respectively. The highest intensity class shows the highest relative increase under longer return periods. This approach enables a large-scale hazard indication assessment based on high-quality input data. The results are a valuable base for further planning and investigations that incorporate climate change. Limitations in the methodology lie in the static definition of release area and deterministic parameterization.

1 Introduction

Debris flows are a type of gravitational mass movements described in Iverson (2014) as "Water-laden masses of soil and fragmented rock that rush down mountainsides, funnel into stream channels and entrain objects in their paths". The moving mass goes through various physical stages (Klubertanz et al., 2009) and surging behavior (Schöffl et al., 2023) as it moves downstream until eventually depositing in lateral levees and a main depositional lobe (Iverson, 2014). A reaction of a channel to extreme precipitation varies on a continuous scale between clear-water flows, hyper-concentrated flow, debris floods and debris flows. Transition between these types can occur through bulking or dilution. Only debris flows have a concrete criterion in that sediment and water are thoroughly mixed (Church and Jakob, 2020). Despite this, debris-flow risk management is fundamentally different from floods due to the different material composition, flow behavior and return period (Davies et al., 2024). Therefore, it is important to make a distinction between the channel response types. Debris flows form a massive hazard throughout mountainous areas in the world due to their fast flow, long runout and poor predictability (Kumar et al., 2024). Three types of debris flow triggers are described in Qie et al. (2025) being (1) short convective storms, (2) long period of rain (3) outbursts from (glacial) lakes. These triggers lead to debris flows as either a cascading hazard (from lake outbursts or landslides on the channel bank) or by in channel mobilization of material as the other example (Hürlimann et al., 2003). Cryospheric debris flows are a special group as they are among the largest and most destructive debris flows in the Alps (Chiarle et al., 2007). Debris flows originating in

glaciated terrain tend to be less sensitive to precipitation intensity than debris flows in lower, non-glaciated regions. The role of sediment processes and availability play a bigger role (Yu et al., 2021).

Debris flow events are among the most destructive gravitational events (Baggio et al., 2024) and can lead to substantial human and economic losses (e.g. Shah et al., 2025). In Switzerland, debris flows cause average annual losses of approximately CHF 321 million between 1972 and 2024 (Federal Office for the Environment (FOEN), 2025). To (cost-)effectively prevent losses, a quantification of hazard is essential. Engineers rely on modelled maximum flow to plan protection measures for infrastructure assets (Kumar et al., 2024). On a global scale, debris flows are expected to become more common (Savina et al., 2020), therefore not only current but also future scenario modelling of debris flow hazard is essential. Debris flow hazard combined with exposure and vulnerability allows for quantitative risk calculations of which hazard modelling is an important building block. Risk calculations should guide planning of adaptation measures and determine acceptable vs. unacceptable risk spatially explicit (Davies et al., 2024). Debris flow initiation and runout are variable through various dimensions and highly dependent on a wide range of characteristics.

Debris flow susceptibility is a concept giving a relative quantification and/or classification of hazard for predefined areas (e.g. Melelli and Taramelli, 2004). From susceptibility, release areas or model start areas are defined, from which debris-flow runout is simulated. In Scheidl et al. (2013) four types of debris-flow runout models are mentioned: (1) expert-knowledge based on historic or geologic evidence (2) physically-based models (3) empirical (statistical) models and (4) statistical models with physical constraints (e.g. grfin tool, U.S. Geological Survey, 2025; Lee et al., 2025). Expert-knowledge and expert-knowledge based models, such as SEDEX, tend to perform well in local analyses (Kienholz et al., 2010). Empirical methods for debris-flow extent and volume can give quick results (Gertsch and Kienholz, 2008), can be spatially explicit (e.g. TopFlowDF, Scheidl and Rickenmann, 2011) and are capable of capturing changing debris-flow behavior through scenario modelling (Baggio et al., 2024). A good example of an empirical method are intensity duration curves for debris flows (e.g. Bernard et al., 2025; Dixit et al., 2024). For larger scales, empirical methods tend to become less reliable and require more complicated corrections (Cavagnaro et al., 2025). Additionally, scenario modelling is not always possible as well as spatially-explicit physical result. Empirical models can be just as good as physically-based models in reproducing past events (Fan et al., 2017). Even as physical model use advances, Iverson (2014) states that empirical models will still have a place in hazard analysis due to their modest data requirement as well as probabilistic capabilities. A probabilistic approach to empirical models, such as DFP (Crescenzo et al., 2024) or MWR (Keck et al., 2024) tend to give good results, despite having a relatively simple statistical flow algorithm. Physically-based models pose an extra challenge as physical variables cannot easily be acquired over large areas (Horton et al., 2013) and therefore empirical models have been preferred. For instance, often, in debris-flow modelling, a correct estimation of material available for transport is more important than the estimation for precipitation and runoff modelling (Kienholz et al., 2010). Another example is the Voellmy approach to fluid behavior, which is widely used in physically based runout models (Bonomelli et al., 2025). This approach is still an approximation requiring parametrization of which the correct parametrization still plays an important role (Yang et al., 2025; Zhang et al., 2022; Graf et al., 2019). Davies et al. (2024) refers to the fact that physical variables will never be perfectly estimated in time and space facts as the "imponderables" and necessitate the use of reference data from true events. Advances and case-studies have however enabled physical models, also over large areas (Graf et al., 2019). An advantage of physically-based models is easily acquiring results other than runout area that can be relevant in hazard/risk analysis, such as flow height, velocity and pressure.

Within the Swiss debris flow hazard modelling community, there are still a multitude of challenges in model choice, model application, model parametrization and model interpretation (Graf et al., 2019). For example, deterministic approaches of regional debris flow hazard analysis under scenarios tend to lead to an over-estimation of hazard (Delmonaco et al., 2003). Therefore in this paper, we aim to be as transparent as possible in our methodological choices, but also in our recommendations for interpretation of the hazard indication maps as well as the shortcomings related to our choices.

Recently, a Large-Scale Hazard Indication Modelling (LSHIM) methodology for snow avalanches in Switzerland has been developed (Bühler et al., 2022), using a tailored version of RAMMS::Avalanche (Christen et al., 2010) that has been applied for further studies in Switzerland (Ortner et al., 2023, 2025b) and in other regions (Fischer et al., 2026; Sykes et al., 2022). This is next to the NAKSIN approach from Norway (Issler et al., 2023), the only large-scale hazard indication simulation approach applying sophisticated avalanche dynamic simulations according to our knowledge. In this manuscript, we aim to emulate this endeavor in developing and applying a LSHIM methodology for debris flow hazard (LSHIM-Debrisflow) and apply it to the Swiss Federal Railway (SBB) infrastructure. Features of LSHIM are the capability of scenario modelling as well as the delineation of release and runout areas. The aims are further developed as follows.

- Develop a national-scale debris-flow susceptibility model using a uniform statistical concept.

– Propagate susceptibility into physically-based runout simulations with RAMMS::LSHIM-Debrisflow (Sect. 5.3) to derive hazard indication maps.

– Produce specific hazard indication maps for return periods of 30, 100, and 300 years suitable for subsequent risk modelling along the Swiss railway network.

Hazard indication and subsequent risk modelling enables adaptation planning. There is a wide range of possible adaptation measures to debris-flow risk. Zimmermann (2004) mentions the establishment of a crisis management committee, evacuation plans, visual monitoring, sensor installation, regular surveys, rain gauge installation and structural measures. Which adaption measure to choose for specific railway infrastructure is outside of the scope of this research, but results presented here will provide a basic guidance to these decisions.

2 Study domain

We produce a national-scale debris-flow hazard indication for the SBB whose network covers large parts of Switzerland. Switzerland is an alpine country (roughly 60 % of the area is covered by the Alps) with a well documented widespread activity of debris flows (Rickenmann and Zimmermann, 1993). Elevation ranges between 193 m in the canton of Ticino up to 4634 m at Dufourspitze in the canton of Valais. Out of the roughly 9.5 million inhabitants, the majority lives in the large bowl between the Alps in the south and the Jura mountain range in the north. Switzerland has a temperate climate, but due to the large altitude differences, it can vary a lot (MeteoSwiss, 2026). In particular, heavy thunderstorms in summer with extreme precipitation peaks can trigger large debris-flow events. Debris flows have been shown to occur not only in the alpine areas but also in the hilly lower elevated parts of the country (Hürlimann et al., 2015). The SBB is the largest railway company in Switzerland that operates fully electrified railway network and serves over a million passengers per day (Swiss Federal Railways (SBB), 2026). Total length of railway lines (excluding tunnels) is 5397 km. This number measures individual railway tracks and does not aggregate parallel tracks. We do not aggregate tracks in the results of this research either. Debris flows have affected the railway infrastructure, for example at the Dornibach, Canton Uri, in 2005 after heavy rainfall (illustrations in Appendix Sect. B1). Such events have led to an ongoing process of increasing resilience at vulnerable sites.

To ensure adequate calculation domains along railway infrastructure, we adopt what are known as "Bilanzgebiete" (singular: Bilanzgebiet) (Bühlmann and Schwanbeck, 2018), i.e. closed catchments of approximately similar size. These are our basic calculation tiles and we added contingency for flow path calculation of a 2000 m buffer, akin to van Zadelhoff et al. (2022). Only debris flows that can reasonably threaten infrastructure are included in the runout calculations by an additional filter of 10 km flow distance from release area to railway infrastructure (excluding tunnels). This threshold comes from the maximum flow length of alpine debris flows as observed by Rickenmann and Scheidl (2010).

3 Swiss hazard and risk framework

We follow the method for hazard mapping in Switzerland, which has been in development since first avalanche hazard maps were issued in the 1960's. The method for avalanches is described in Bundesamt für Forstwesen (BFF) and Eidg. Institut für Schnee- und Lawinenforschung (SLF) (1984), for mass movement hazards in BAFU (2016) and for flood hazards, which include debris flows, in Loat and Petrascheck (1997). The general procedure for risk assessment based on this methodological framework is described in Bründl et al. (2009). It is based on the definition of the return period of initial conditions, which typically include a 30, 100, and 300-year return period and an additional overload scenario with a return period up to 1000 years.

For each of the return period scenarios, the physical impact of debris flows is characterized by the maximum flow height, which is considered the standard both in Switzerland SIA (2020), but also internationally (e.g. Hürlimann et al., 2006). Areas, where the maximum flow height $d_{\max}$ is below 0.5 m are denoted as low intensity, as medium for $0.5\,\mathrm{m} < d_{\max} \leq 2\,\mathrm{m}$, and as high for $d_{\max} > 2\,\mathrm{m}$. We comply with this concept and use the maximum flow height in three intensity classes (see Sect. 5.6) as an indicator for the hazard.

Debris flow hazard in this paper is described with a hazard indication map with return periods of 30, 100, and 300 years. We omit a 1000 year since no reliable precipitation data is available. Hazard indication maps are based exclusively on numerical modelling and do not include a detailed analysis of incident records and field surveys. They are suitable for indicating areas of hazard, but not as a basis for long term land-use planning. As our aim is to indicate hazard hot spots along the entire SBB rail network, we decided, for reasons of practicality, to elaborate hazard indication maps based on the current climate conditions as of 2025 along the railway infrastructure. Recently, probabilistic modelling of alpine mass movements has been introduced by Kleinn et al. (2024) for snow avalanches, as well as for rock fall and shallow landslides for the pilot region in Adelboden, Switzerland (Kleinn et al., 2025). Model results suggest a more differentiated picture than it is obtained with the deterministic approach based on three defined return periods of release conditions. However, due to requirements by the project partner in this study, we comply with the deterministic approach widely implemented in the Swiss natural hazard community.

4 Data

An overview of data sourced and applied in this research is given below. Full details, with references, are given in the Appendix. All data processing is performed with Arcpy in the ArcGIS Pro environment (Esri, 2024).

4.1 Topography

Our basic DEM is the LiDAR-based SwissALTI3d (Federal Office of Topography swisstopo, 2024c) at a 0.5 m resolution. We resample to 1 m and compute flow accumulation, slope, curvature and aspect as well as catchment delineation for the susceptibility analysis (Sect. 5.2). In distributed runout modelling, DEM resolution plays an important role. In Stolz and Huggel (2008), a 25 m is considered too coarse for a typical debris flow channel in Switzerland making it unable to replicate the existing channel. A 4 m resolution is deemed sufficient. For computational reasons we settle on a 5 m resolution with cubic resampling.

4.2 Landscape data

The susceptibility analysis (Sect. 5.2) takes into account the spatial distribution of binary forest cover data, vegetation height, various geological layers as well as geomorphological layers (see Appendix Table A2).

4.3 Cryosphere

Current permafrost extent is extracted from PGIM (Kenner et al., 2019). All permafrost classes, whether continuous or discontinuous, are treated as permafrost presence. SGI2016 (Linsbauer et al., 2021) provides a complete glacier inventory for Switzerland, which is treated as binary glacier presence map.

4.4 Extreme precipitation

Extreme precipitation, for application see Sect. 5.4, at 1 h duration at 30-, 100-, and 300-year return period interval is sourced from the MeteoSchweiz spatially distributed intensity-duration product (Fukutome et al., 2023). Surface area correction of extreme precipitation applies the methodology of Grebner et al. (1999).

4.5 Event inventory for model training

Debris flow propagation is a complex process and does not always have a clear initiation, transport, and deposition area (e.g. Simoni et al., 2020; Cannon et al., 2003). For this reason we use the StorMe debris flow inventory polygon data (see Appendix Table A2) that identify process domains, rather than fixed points. Inventories of past events suffer from biases and methodological inaccuracies, especially over larger areas. Additionally, we often do not know how exceptional recorded events are (Graf et al., 2019; Stoffel et al., 2005), but the StorMe inventory is the best reference data set to our knowledge. We have a total of 6351 debris flow polygons as well as 19 175 flood polygons, that are applied as explicit absence polygons.

5 Methods

The general workflow for the LSHIM debris flow framework with both susceptibility and runout is shown in Fig. 1. Details for the analysis in the specific sections.

5.1 Potential release areas

We focus on debris flow that originate from bulking. This excludes large magnitude single-events from glacier collapse, GLOFs or large landslides. For bulking types, the initiation should not be thought of as a specific point in a channel, but rather a zone where initiation varies due to local heterogeneity in extreme precipitation and sediment availability (Yamanoi et al., 2025; Hürlimann et al., 2003). Observations on release areas are slopes steeper than about 25–30° (Iverson, 2014) and, based on California debris flows, flow accumulation between 0.2 and 1 km^2 (McGuire et al., 2023; Struble et al., 2023). Our methodology defines potential debris flow channel sections as sections, where the flow accumulation is between 0.1 and 2 km^2. The broad range is deliberate and anticipates subsequent filtering (Sect. 5.2).

Specific release points in the susceptible channel, i.e. Potential Release Areas (PRAs, singular: PRA), are a model necessity. We approximate the natural variation in initiation zones by allowing multiple PRAs to be defined along the length of a susceptible channel section. We place a point along the channel at a fixed interval of 750 m. This interval is qualitatively chosen to balance the computational burden with the heterogeneity of properties in the channel. In this research, we assume static sediment availability through time. This contrasts with variable sediment availability (Gertsch and Kienholz, 2008), which is closer to reality, but for computational efficiency, we decided on a general solution.

5.2 Susceptibility modelling

Statistical debris-flow susceptibility analysis from a range of relevant landscape properties (topographical, hydrological, geological, vegetation) is a tried-and-tested method (e.g. Liu et al., 2025; Morel et al., 2023; Napoli et al., 2023; Shen et al., 2017; Kim et al., 2016; Melelli and Taramelli, 2004). Generally, a diverse set of properties increases accuracy (Kritikos and Davies, 2015), since many factors influence debris-flow initiation (Marchi et al., 2019) or vary locally (Morel et al., 2023). For instance, the intuitive relationship between catchment area and debris flow occurrence is only very weak in a comparison of 809 debris flows in northeastern Italy, but multiple properties of specific stream sections and their catchments is a good predictor of debris-flow initiation and

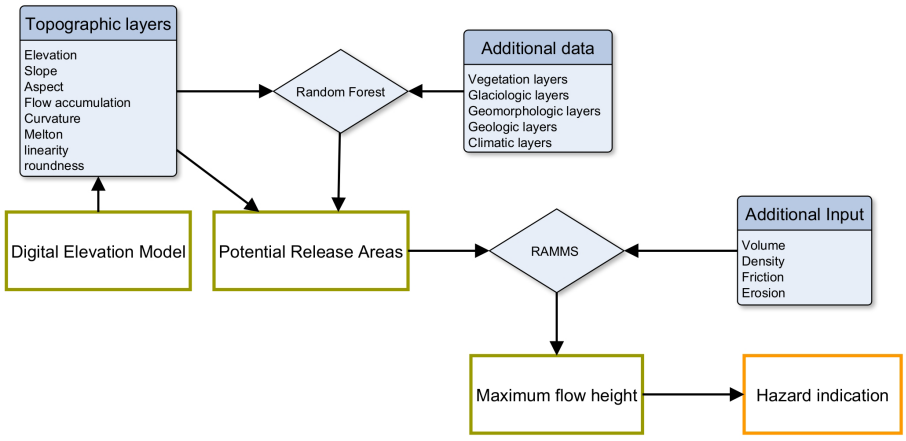


Figure 1. Flowchart of the general methodology for debris-flow susceptibility and runout analysis.

even dimensions (Kienholz et al., 2010; Miller and Burnett, 2008). Using only raster properties does not do justice to the processes involved in debris flow generation, rather a focus should be on features (Liu et al., 2025; Melelli and Taramelli, 2004) or catchment-based properties (Lee et al., 2025).

In addition to properties from a potential discrete source point, we take into account properties of the channel and the catchment that flow into the source point. This gives a total of 41 properties that are displayed in Appendix Table A3. Reference PRAs are defined by overlap with the StorMe inventory (Sect. 4.5) for debris flows (presence points, $n = 2490$) and floods (absence points, $n = 814$). Model training is performed using a set of candidate algorithms: random forest (Breiman, 2001), logistic regression (Harris, 2021), CatBoost (Prokhorenkova et al., 2018), naive Bayes (Zhang, 2004), XGBoost (Chen and Guestrin, 2016), support vector machine (Drucker et al., 1996), and a simple neural network (Goodfellow et al., 2016). All models are implemented in Python using the scikit-learn package (Pedregosa et al., 2011). To select a model, we test all using the reference PRAs with a 10-fold cross validation. Model application results in a PRA-specific debris flow vs. flood probability, $P_{\text{Debris flow}}$, between 0 and 1.

5.3 Runout modelling with RAMMS

The RAMMS software has been used for modelling of gravitational processes in many studies worldwide (Kumar et al., 2024). Our version of RAMMS, RAMMS::LSHIM-Debrisflow, (RAMMS AG, 2024) (hereafter also referred to simply as RAMMS) is tailored for large-scale application to run simulations for groups of PRAs. RAMMS does a pre-run to narrow down the calculation domain. The pre-run resolution is 10 m. Results are then generated at a 5 m resolution. The initial domain is defined by a buffered (750 m) downstream line from the PRA. Upon reaching the first flat channel section ($< 4°$ for > 250 m), we define the assumed cone neck point and apply a 1750 m buffer.

5.4 Hydrograph volume and discharge parameterization

Correct estimates for hydrograph total volume and peak discharge are part of parameterization (RAMMS AG, 2024). It is important as both entrainment and eventual runout modelling are sensitive to hydrograph dimensions (Frank et al., 2017). In our one-phase approach, hydrograph volume (V_{total}) consists of a mixture of water and sediment. We relate the total water volume (V_{water}) to the catchment area ($A_{\text{catchment}}$) in m^2, a runoff coefficient (unitless), r, and the 1 h extreme precipitation ($P_{1\,\text{h}}$) in m, according to Eq. (1) below. Hirschberg et al. (2019) indicates the huge variety in runoff coefficient over 52 observed debris flows. To simplify, we settle on a default value 0.1.

$$V_{\text{water}} = A_{\text{catchment}} \cdot P_{1\,\text{h}} \cdot r \tag{1}$$

Glacial presence in the catchment area of a stream slows the reaction time of the catchment to extreme precipitation (e.g. Klok et al., 2001) as the accumulation zone of glaciers work as a long-term buffer. The ablation zone displays quicker runoff (Jansson et al., 2003). We assume as general rule that 2/3 of the glacier is the accumulation zone, 1/3 is ablation zone. We compute the degree of glaciation in a PRA catchment and assume the glacier accumulation zone of a catchment has a runoff coefficient of 0.0. This is in accordance with the assumed buffer capacity. The ablation zone, as well as the non-glaciated part have the default value. The proportional average of the parts give an adjusted runoff coefficient.

We assume 1 h is a representative approximation of the time to concentration for our catchment dimension. The order of magnitude is supported by the review paper by Beven (2020) and the 1 h duration is convenient in terms of

data availability. Applications in comparable research vary widely, with McGuire et al. (2024) using a 15 min intensity, seasonal dependent 10–40 min in Iadanza et al. (2016), 10 min to 24 h in Hirschberg et al. (2021) and Rickenmann et al. (2008) using 72 h. All above imply an assumption on the type of debris flow in their respective case studies. On a national scale, we want to include multiple types of debris flows through assumed density of the flow material in our one-phase approach. This is relevant for the hydrograph volume as well as debris-flow pressure calculation in RAMMS. Using a factor to amplify discharge volume based on assumed debris-flow type has been successfully applied in Cavagnaro et al. (2024). The range of observed debris flows in Switzerland is from smaller watery muddy debris flows to large granular debris flows (Davies, 1997). Predictions on which type of debris flow occurs when and where is still challenging (Graf et al., 2019). According to the SIA norm (SIA, 2020), density of Swiss debris flows varies between 1400 (fluid flows) and 2100 (granular flows) $\mathrm{kg\,m^{-3}}$. We assume that $P_{\text{Debris flow}}$ (Sect. 5.2) correlates with the density of the debris flow, $\rho_{\text{debris flow}}$, according to Eq. (2) below.

$$\rho_{\text{debris flow}} = 1400 + (700 \cdot 2 \cdot (P_{\text{Debris flow}} - 0.5)) \quad (2)$$

The normalization with 0.5 is because for PRAs with $P_{\text{Debris flow}} < 0.5$ floods are more likely and these are not considered debris flow prone. Hydrograph volume, V_{total}, is attained by combining water volume and debris-flow density through Eq. (3) below.

$$V_{\text{total}} = V_{\text{water}} \left(1 + \frac{\rho_{\text{debris flow}} - \rho_{\text{water}}}{\rho_{\text{sediment}} - \rho_{\text{debris flow}}}\right) \quad (3)$$

Here ρ_{water} is the water density at $1000\,\mathrm{kg\,m^{-3}}$ and ρ_{sediment} is sediment density at $2500\,\mathrm{kg\,m^{-3}}$. Maximum discharge in the hydrograph, $Q_{\max}$, is related to total volume using the empirical relationship from Rickenmann (1999) given in Eq. (4) below.

$$Q_{\max} = 0.1 \cdot V_{\text{total}}^{\frac{5}{6}} \quad (4)$$

5.5 RAMMS parametrization

As with many other models, parametrization of processes is important. Flow direction and height is calculated by solving the shallow water equations (Bonomelli et al., 2025). Additionally the Voellmy approach, which simplifies friction behaviour, governs flow behavior and runout extent (Salm, 1993). The basic equation with parameters is given in Eq. (5) below. The complete RAMMS approach which additionally includes yield-stress and curvature dependent contribution is described in RAMMS AG (2024).

$$S = \mu N + \frac{\rho g \parallel u \parallel^2}{\xi}, \quad \text{with} \quad N = \rho h g \cos\varphi \quad (5)$$

S is the basal shear stress [Pa], μ is the Coulomb friction coefficient, ξ is the turbulent (viscous) friction parameter

Table 1. Classification of TLM, GeoCover, and erosion classes. "Altschutt" comprises rock debris that has undergone substantial weathering, whereas "Jungschutt" consists of fresh to only slightly weathered material. Note: The erosion class is reduced by one level within the *Kristallin* tectonic unit.

TLM class	Altschutt/Jungschutt	Erosion class
Rock	Altschutt	Low
Unconsolidated material	Altschutt	High
Other	Altschutt	Medium
Rock	Jungschutt	None
Unconsolidated material	Jungschutt	Medium
Other	Jungschutt	Low

$[\mathrm{m\,s^{-2}}]$. Back-calculated μ has a value between 0.01 and 0.3, ξ between 100 and 1000 (Zimmermann et al., 2020). ρ is the bulk density of the flow $[\mathrm{kg\,m^{-3}}]$, g is the acceleration due to gravity $[\mathrm{m\,s^{-2}}]$, u is the depth-averaged velocity vector $[\mathrm{m\,s^{-1}}]$, h is flow height [m], φ is the slope angle [°]. The Voellmy approach simplifies friction to two coefficients, namely μ and ξ. Of these, ξ governs flow behavior and μ, basal friction, governs stopping behavior of the debris flow (Naqvi et al., 2025; Rickenmann and Scheidl, 2023). The importance of correct parametrization of friction, especially μ is stressed in many projects (Kumar et al., 2024; Scheidl et al., 2013). In general, ξ has little influence on debris-flow extent (Bolliger et al., 2024). For computational reasons, interpretability, and the risk of equifinality with additional dimensions of variation, we decide to spatially parametrize μ and define a constant value for ξ ($300\,\mathrm{m\,s^{-2}}$). μ is approximated by the tangent of the angle of deposition (Bolliger et al., 2024), which in turn is approximated by the slope angle in 11 076 identified debris-flow fans in Federal Office of Topography swisstopo (2024a). The angle of deposition of material is dependent on local to regional geological properties. We aggregate deposition angle per Bilanzgebiet. A range of percentiles (50th, 30th, 10th and 5th) was constructed and compared to previous local applications for RAMMS. For example, 0.05 at Illgraben, Canton Valais (Bolliger et al., 2024; Berger et al., 2011) and 0.20 at Spreitgraben, Canton Bern (Frank et al., 2015). After multiple tests, we settle on the 5th percentile of the slope angles of fans present within the Bilanzgebiet. To prevent outliers, we apply two postprocessing steps. Firstly, we only parametrize Bilanzgebiete if at least 10 fans are present. Secondly, we apply a moving-window smoothing. The trade-off of this method is that local variability is reduced, but in turn we have a more complete and reliable large-scale friction parametrization. We assessed window sizes of 5, 10, 15, and 20 km and settled on 10 km for the best trade-off. The spatial distribution is given below in Fig. 2a, which will serve as input to RAMMS.

Often the initial debris flow volume is small, but becomes multitudes larger (Shen et al., 2020 found 4–20 times larger)

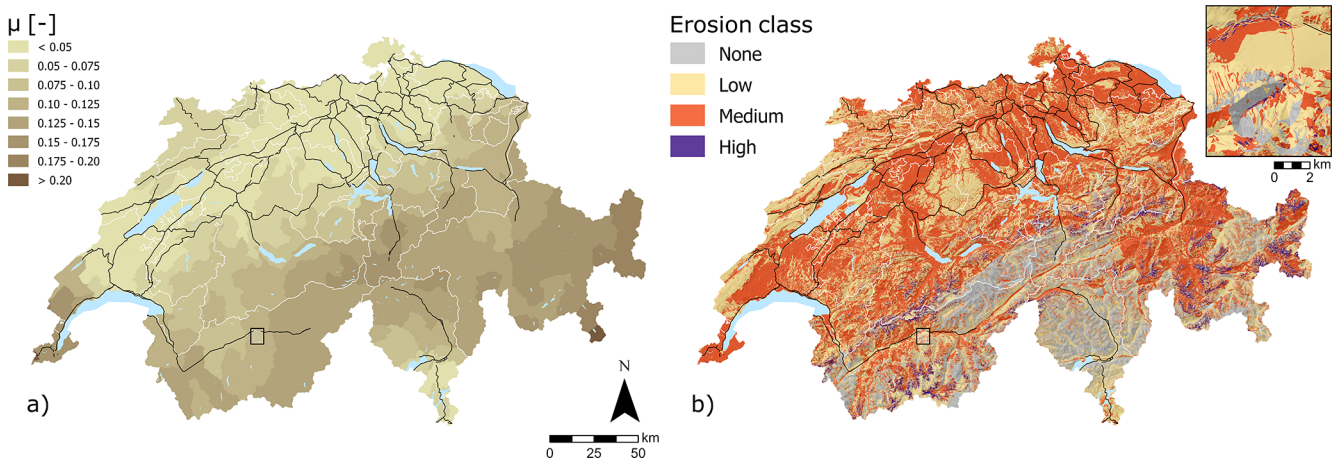


Figure 2. (a) Spatial distribution of the Voellmy μ parameter over the Bilanzgebiete based on the slope angle of documented debris-flow fans and a moving-window smoothing algorithm. **(b)** Erosion classes for Switzerland based on the decision scheme in Table 1. The square indicates the extent of the detailed map of the Illgraben area (canton of Valais). SBB infrastructure is displayed in black, cantonal boundaries in white.

due to entrainment of material along the way down (Berger et al., 2011). This indicates that a good assessment of available material and entrainment capacity is absolutely necessary and needs to be applied in addition to the original hydrograph volume (Eu and Im, 2025; Shen et al., 2020; Kienholz et al., 2010). RAMMS includes a spatially explicit entrainment module, giving it an edge over many other runout models (Kumar et al., 2024). In Frank et al. (2017), it is noted that the entrainment module in RAMMS works well, but more case studies are needed.

The RAMMS erosion module includes five parameters: (1) erosion density [$\mathrm{kg\,m^{-3}}$], describing the density of the erodible material; (2) erosion rate [$\mathrm{m\,s^{-1}}$], controlling the rate at which material is entrained from the bed; (3) potential erosion depth [$\mathrm{m\,kPa^{-1}}$], relating erosion depth to applied shear stress; (4) critical shear stress [kPa], defining the threshold above which erosion can occur; and (5) maximum erosion depth [m], limiting the thickness of erodible material (RAMMS AG, 2024). At the national scale, a spatially explicit parameterization of all five parameters is not feasible. We therefore assume a spatially uniform erosion density ($2000\,\mathrm{kg\,m^{-3}}$), while the other parameters are defined for four distinct erosion classes: *None*, *Low*, *Medium*, and *High*. These classes are assigned using a decision scheme based on TLM land cover (Federal Office of Topography swisstopo, 2024b), GeoCover tectonic units, and topographic characteristics (Table 1). For the geological classification, we apply the concepts of "Altschutt" and "Jungschutt" (Gertsch and Kienholz, 2008) to the GeoCover units. "Altschutt" represents older material that has undergone substantial weathering, whereas "Jungschutt" comprises fresh to only slightly weathered material. The resulting spatial distribution of erosion classes is shown in Fig. 2b.

Erosion classes are used to parametrize RAMMS through three physical erosion parameters (Table A4) and available sediment (Table A5), which also is a function of return period. The *medium* erosion class corresponds to the default RAMMS erosion parameterization, which is based on observations from the Illgraben catchment (RAMMS AG, 2024). As no established framework exists for representing spatially heterogeneous RAMMS erosion parameters at regional to national scales, the *low* and *high* classes are defined relative to this reference. Based on exploratory model testing, parameter values are set to half of the default values for the *low* class and twice the default values for the *high* class. Areas classified as *no erosion* are assigned a potential erosion depth of zero, thereby preventing entrainment. This classification provides a consistent representation of spatial variations in erosion potential at the national scale, but constitutes a simplification of local erosion processes. In particular, the scaling factors distinguishing the erosion classes are empirically defined rather than independently calibrated.

5.6 Hazard indication map generation

The output of RAMMS is a spatially explicit data set for each of the considered 30-, 100-, and 300-year return period scenario including spatially explicit intensity information such flow height, flow velocity, flow pressure, flow momentum and erosion (RAMMS AG, 2024), of which the maximum flow height was used to categorize intensity into the three intensity classes low, medium and high according to the method of hazard mapping (see Sect. 3). Areas in which the modelled maximum flow height d_{max} was below 0.01 m were omitted from the analysis to exclude negligible modelled flow depths and numerical spreading at the margins of the simulated runout. The threshold was chosen in

accordance with other applications of RAMMS (e.g. Hauser, 2011).

6 Results and interpretation

6.1 Susceptibility model performance and predictors

Results on selected metrics of our susceptibility models are displayed in Table 2. Given the goal of planning measures and allocating resources, both false positives and false negatives are to be avoided in equal measure. For this reason accuracy and ROC-AUC are chosen as primary measures. The random forest model performs best on both measures and we apply it for further susceptibility analysis. It must be noted that between machine learning techniques differences are small and variation around the mean performance is greater than the difference between models, rendering any of these models a valid choice. Neural network and support vector machine also perform well. Optimizing models is outside of the scope of this research, but given extensive calibration, we can see these models attaining similar performance to machine learning techniques. Naive Bayes favors recall over discrimination ability, resulting in a skew with many false positives. The opposite is true for logistic regression, which has a conservative classification judging for low recall but high precision. This indicates debris-flow susceptibility is not easily predicted by linear models and involves complex interactions that are better represented by any of the other models.

Detailed information on the random forest relative attribute importance is shown in Fig. 3 below. Most influence is exerted by attributes related to precipitation and topography with an additional role for geology, geomorphology and vegetation. Also the low magnitude of parameter influence suggest sufficient overlap and coverage by the attributes.

A final random forest model is retrained on the entire reference dataset and applied to all PRAs with a predicted debris-flow probability for each PRA ($P_{\text{Debris flow}}$) shown in Fig. 4a. A detailed view of the well-known Illgraben area is shown for reference. The resulting probability ranges from 0 to 1 (or 0 %–100 %) where values approaching 0 % indicate that an event is more likely to be classified as a flood and values approaching 100 % indicate that it is more likely to be classified as a debris flow. The continuous predicted probability is converted to a binary classification split at 0.5, where both debris-flow and flood are equally likely. This creates points classified as debris-flow prone ($P_{\text{Debris flow}} \geq 0.5$) and points classified as flood prone ($P_{\text{Debris flow}} < 0.5$). The initial 80 812 PRAs are filtered based on proximity to the railway infrastructure resulting in a total of 16 756 PRAs for runout analysis (Fig. 4b).

6.2 Runout modelling

Runout from PRAs, conditionally parametrized with precipitation and erosion capacity on a return period, is modelled dynamically with RAMMS. Given versatility and the physical basis of RAMMS, we model runout from PRAs at discrete timesteps with an explicitly distributed flow height, flow velocity and pressure. This is shown for the well-known Illgraben area in Fig. 5. Entrainment erosion is also explicitly computed every timestep. In the example, as with many debris flows, a multitude of mobilized material is generated through entrainment compared to the initial volume.

As maximum flow height of a debris flow through all timesteps is the standard for Swiss debris-flow risk analysis (Sect. 5.6), we display this as a national scale through the country and under specific return periods in Fig. 6. To highlight modelling influence, We focus on three example areas with a distinct area namely the pre-alpine Emmental, alpine but sediment-limited Ticino and alpine cryosphere-influenced Valais. A benefit of using maximum flow height is that we incorporate overlapping paths of debris flows and implicitly choose the most hazardous. Details on selected study areas are given in Table 3.

Figure 6 shows a consistent increase in debris flow maximum flow height through all study areas under more extreme scenarios, which is directly related to the more extreme 1 h precipitation. The difference is notably less pronounced in the sediment-limited area of Ticino. This is highlighted in the histogram of flow heights categories as shown in Fig. 7 below.

The difference between example areas, shows the strong increase in affected area under the more extreme 300-year return period scenario compared to the 30-year scenario and to a lesser degree the 100-year scenario. This also indicates that the extreme precipitation value works through the model architecture and increases affected area with more extreme scenarios.

6.3 Hazard indication mapping

Maximum flow height forms the basis for hazard indication mapping as described in Sect. 5.6, which is displayed in conjunction with Fig. 6 in Fig. 8.

From Fig. 8 we conclude that the total length of affected SBB railway increases significantly when comparing a 30-year return period with both a 100 (+39 %) or 300-year (+56 %) return period. This is in line with the maximum flow height results from Fig. 7. Interesting to note is that the absolute increase in the lower hazard category is modest. More significant increases are seen in affected railway at second or third intensity. Compared to the entire railway infrastructure, approximately 1.6 % of railway length is threatened by debris flows under the 300-year return period.

Table 2. Mean and standard deviation of performance metrics from a 10-fold cross validation of selected statistical models in predicting debris-flow susceptibility. All models use standard parametrization.

	Accuracy	ROC-AUC	Precision	Recall	F_1 score
random forest	0.814 ± 0.016	0.866 ± 0.021	0.820 ± 0.014	0.967 ± 0.012	0.887 ± 0.009
XGBoost	0.812 ± 0.015	0.841 ± 0.022	0.837 ± 0.012	0.933 ± 0.015	0.882 ± 0.009
CatBoost	0.812 ± 0.014	0.833 ± 0.025	0.824 ± 0.009	0.954 ± 0.015	0.884 ± 0.009
support vector machine	0.810 ± 0.013	0.825 ± 0.021	0.817 ± 0.010	0.963 ± 0.015	0.884 ± 0.008
neural network	0.802 ± 0.023	0.815 ± 0.029	0.859 ± 0.018	0.882 ± 0.019	0.870 ± 0.015
naive Bayes	0.778 ± 0.008	0.627 ± 0.041	0.788 ± 0.007	0.965 ± 0.008	0.867 ± 0.004
logistic regression	0.710 ± 0.032	0.784 ± 0.018	0.879 ± 0.010	0.713 ± 0.046	0.787 ± 0.029

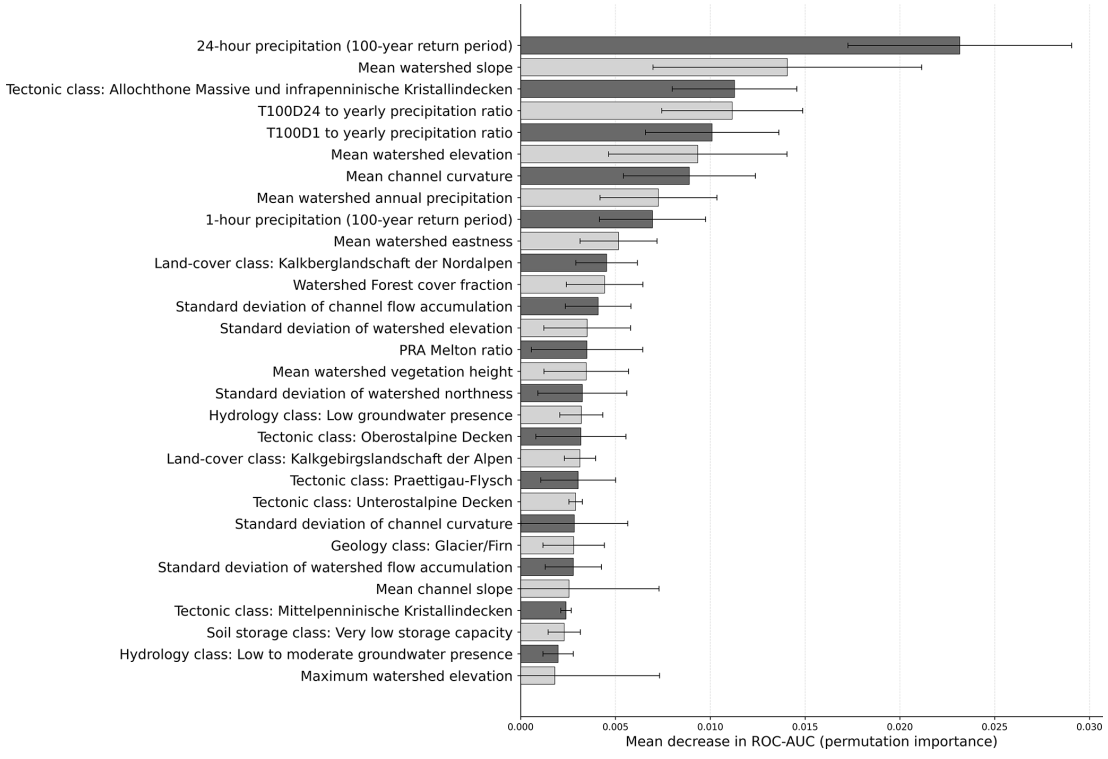


Figure 3. Random forest mean input parameter importance quantified by mean decrease in ROC-AUC by removal of the target attribute. Only the 30 most important features are shown. Classified data applies the majority class in a PRA watershed.

7 Discussion

7.1 Implications for railway hazard and risk management

Hazard and risk mapping over larger areas, such as regions or whole countries has gained increasing interest among natural hazard professionals in the last 20 years. It offers the possibility to get an overview about hazards in areas, where no other information such as hazard maps is available. The difference between a hazard indication and hazard map being that the latter requires local expert knowledge and can entail legal constraints. Bühler et al. (2022) gives a brief overview on approaches since 2004 and presents a method for an automated hazard indication modelling of snow avalanches for the Canton of Grisons in Switzerland. This work represents the basis for the multi-hazard risk framework of Ortner et al. (2023), who simulated potential developments of avalanche risk to buildings driven by climate change in central Switzerland (Ortner et al., 2025a, b). Comparable and recent approaches are presented by Issler et al. (2023) for Norway and by Fischer et al. (2026) for Alaska.

Since then these approaches have been applied in large-scale modeling of rockfall (Bründl et al., 2025) and debris flow (this paper). For natural hazard professionals, responsible for the safety of public infrastructure such as the SBB, large-scale hazard and risk mapping offers the opportunity to identify areas with elevated hazard or risk and thereby

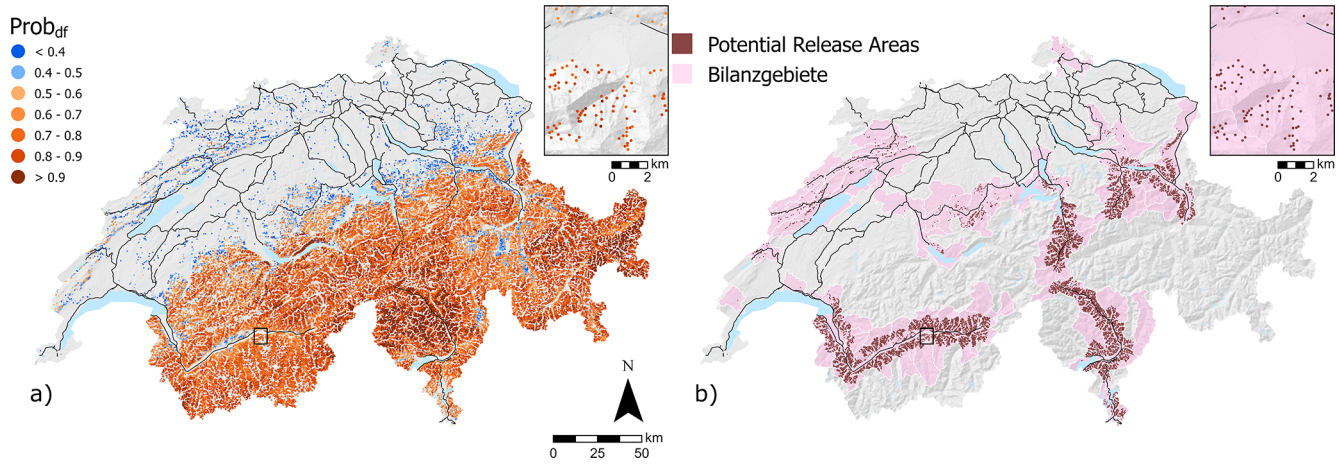


Figure 4. **(a)** Debris-flow susceptibility at hydrograph points, expressed as the probability predicted by the random forest model. **(b)** 91 Bilanzgebiete and 16 756 Potential Release Areas within reach of SBB railway infrastructure included in RAMMS. For both subfigures, a detailed view of the well-known Illgraben area is shown for reference.

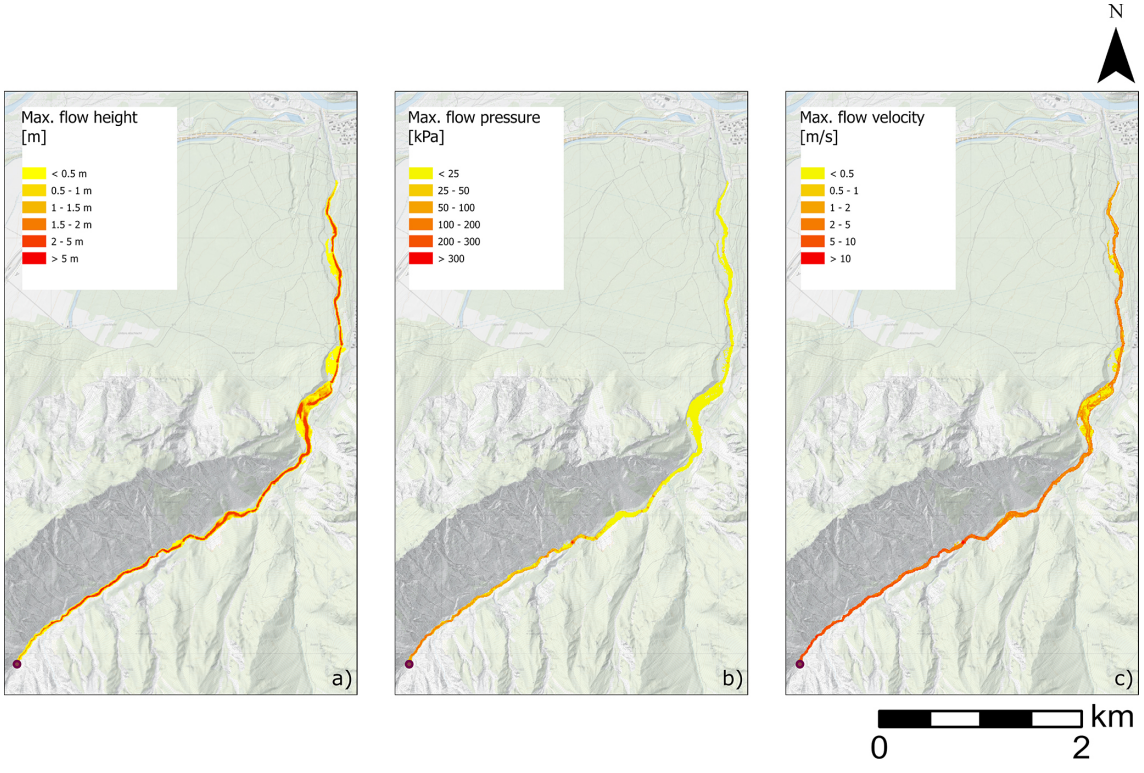


Figure 5. Example of RAMMS model results showing a debris flow from a single PRA (in purple) in the Illgraben catchment (Canton Valais) modelled under a 100-year return period. This debris flow has an initial volume, V_{total}, of 3648 m^3. Assumed density, $\rho_{\text{debris flow}}$, is 1761 kg m^{-3}. Total mobilized material volume is 75 713 m^3. Simulated time of the event is approximately 46 min. Through all timesteps **(a)** the maximum flow height, **(b)** the maximum flow pressure, and **(c)** the maximum flow velocity.

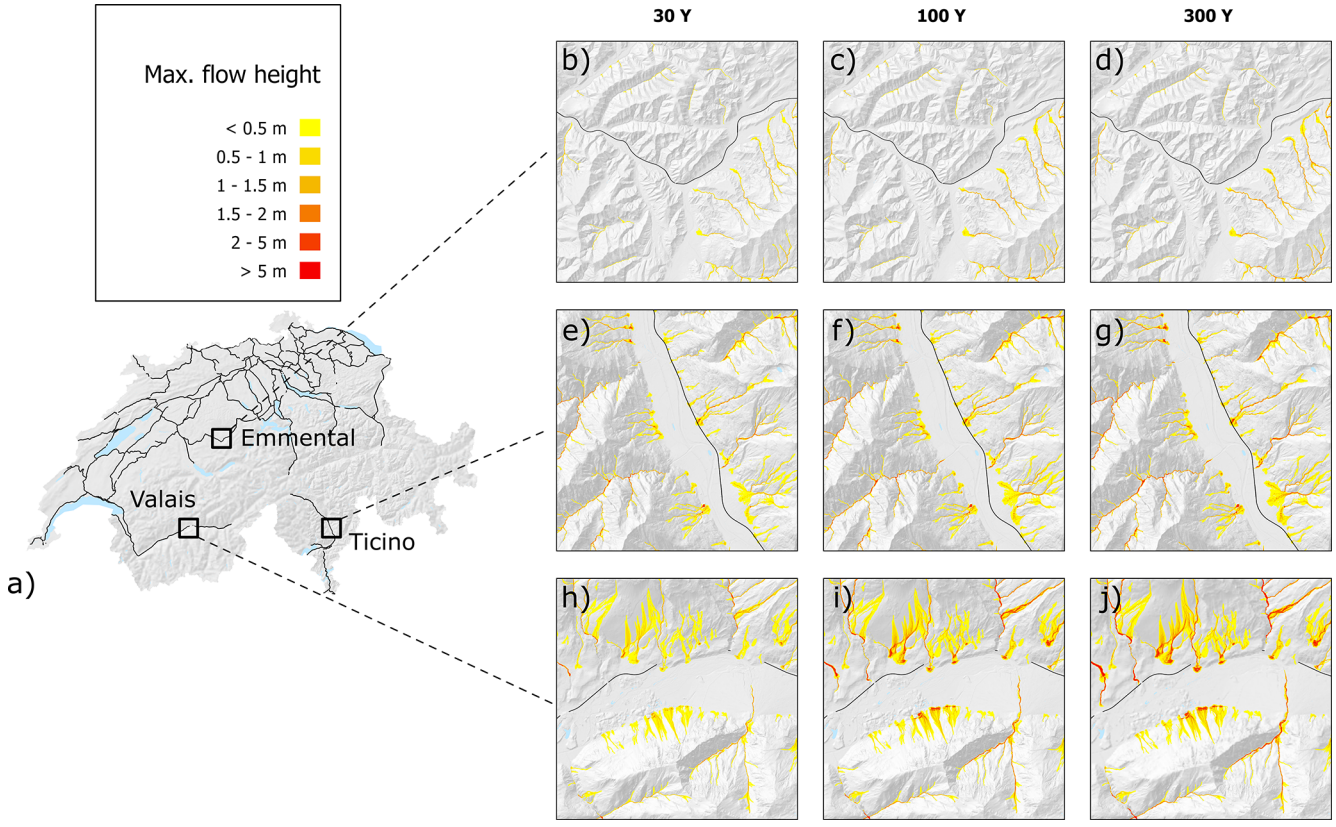


Figure 6. Debris flow maximum flow height for selected example areas along the SBB railway track (black lines) under a 30-, 100-, and 300-year return period. **(a)** National-scale overview. Emmental for **(b)** $T = 30$ years, **(c)** $T = 100$ years, **(d)** $T = 300$ years. Ticino for **(e)** $T = 30$ years, **(f)** $T = 100$ years, **(g)** $T = 300$ years. Valais for **(h)** $T = 30$ years, **(i)** $T = 100$ years, **(j)** $T = 300$ years.

Table 3. Summary statistics for three example areas. All areas are of identical size (110 km^2). Erosion gives the percentage of the area per class.

Environment		Emmental	Ticino	Valais
		Pre-alpine	Sediment-limited	Inner-alpine
PRAs	No.	57	367	326
Mean PRA elevation	m a.s.l.	1076	1124	1240
Mean debris-flow bulk density	$kg\,m^{-3}$	1527	1974	1726
Mean μ	–	0.07	0.11	0.11
Mean 30-year 1 h rainfall	mm	55	63	25
Mean 100-year 1 h rainfall	mm	72	81	32
Mean 300-year 1 h rainfall	mm	90	100	40
Erosion class No erosion	%	0	56	11
Erosion class Low	%	70	42	54
Erosion class Medium	%	30	2	34
Erosion class High	%	0	0	1

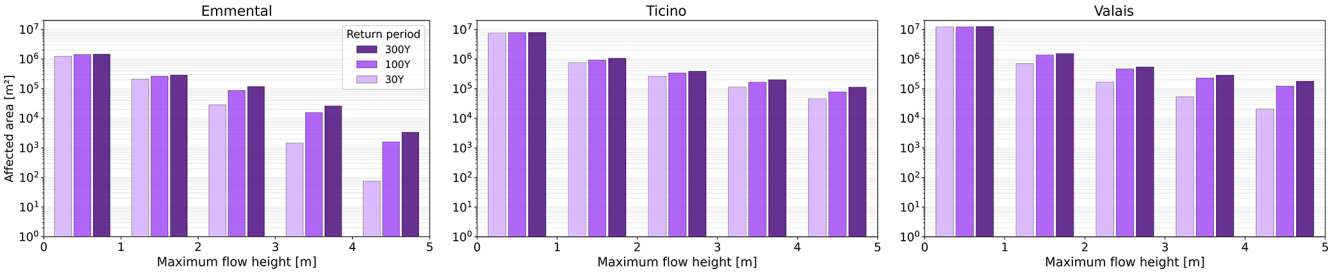


Figure 7. Histograms of affected area at 1 m interval of maximum flow height for three example areas from Fig. 6. Bars display the 30-, 100-, and 300-year return period. Note the logarithmic scale.

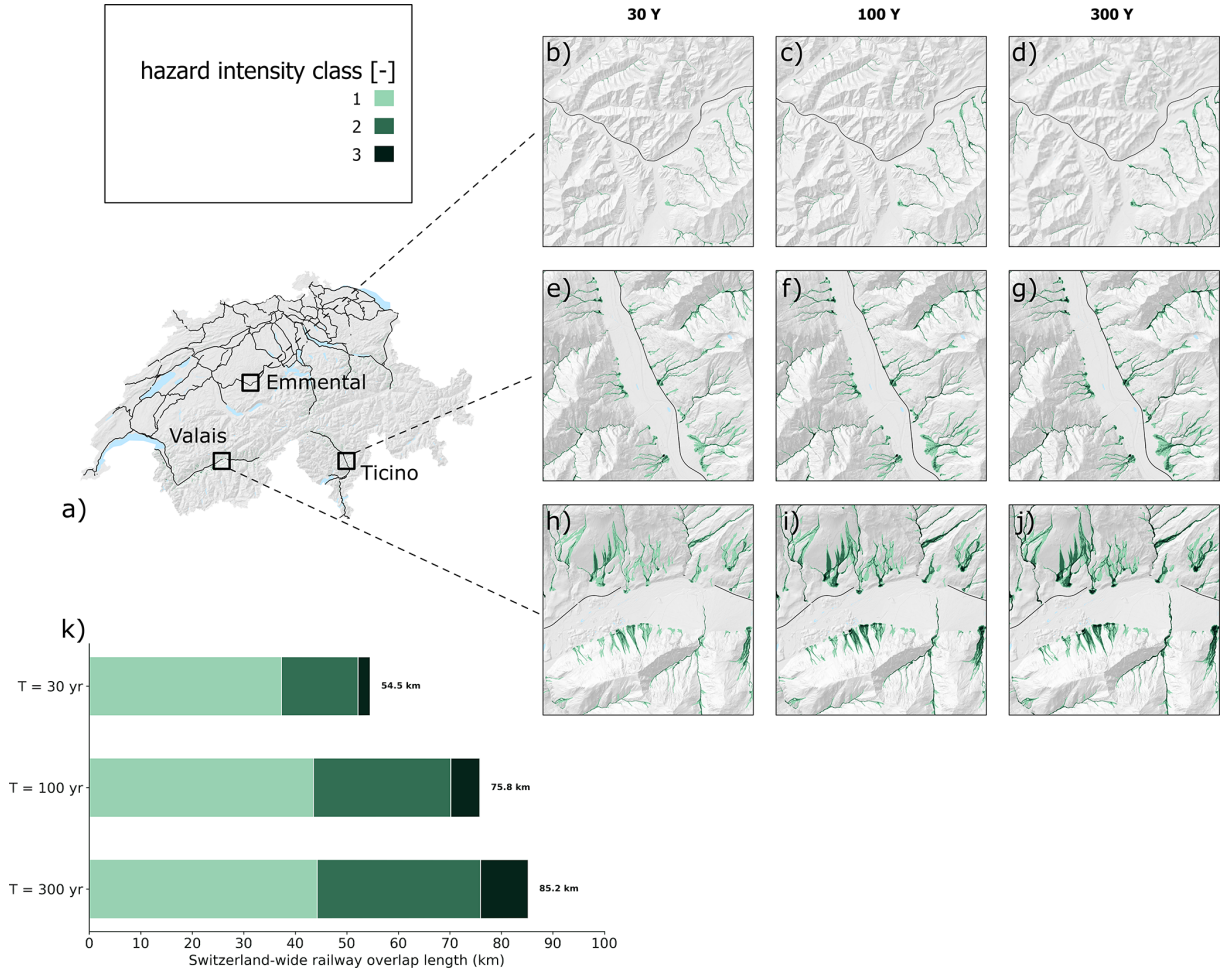


Figure 8. Hazard indication by intensity at the national scale for three example areas. **(a)** national-scale overview. Emmental for **(b)** $T = 30$ years, **(c)** $T = 100$ years, **(d)** $T = 300$ years. Ticino for **(e)** $T = 30$ years, **(f)** $T = 100$ years, **(g)** $T = 300$ years. Valais for **(h)** $T = 30$ years, **(i)** $T = 100$ years, **(j)** $T = 300$ years. **(k)** Switzerland-wide length of affected railway subdivided by category.

information, where to prioritize mitigation measures in the future. The results of this study show that a national application to debris-flow hazard can also be achieved and provide general indications for further detailed studies. The results, however, need to be validated and interpreted regarding the consequences of model assumptions and uncertainties.

7.2 Uncertainty and limitations

In our susceptibility analysis, a mean accuracy of 0.814 combined with the proclivity of random forest to overfitting, indicates not every PRA is correctly classified. Runout behavior of small and large debris flows is fundamentally different (Davies, 1997). Though we do a dimensioning of

debris flows (Sect. 5.4), the physical processes in multi-phased over-saturated fluids cannot be captured in our one-phase application of RAMMS. As a single-phase bulk-flow model, RAMMS cannot explicitly represent solid-fluid phase separation, dilution or transitions between debris-flow and debris-flood regimes. Consequently, highly fluid or rapidly transforming flows may not be reproduced adequately without case-specific calibration. Erosion parameterization is not constant and easy to be put in classes or return periods. It varies through time and also depends on debris flow characteristics as well as saturation degree (Roelofs et al., 2023). Case-studies have attempted statistical modelling of entrainment capacity (e.g. Abancó and Hürlimann, 2014), in a manner comparable to our susceptibility model. In scenario modelling and our physical approach, this was not feasible.

We settled on a 1 h reference duration for our extreme rainfall events. Sources in Sect. 5.4 mention the importance of specific catchment characteristics, season, rainfall event shape and antecedent moisture, all of which influence the time of concentration as subsequent reference duration. Our simplification is a compromise and clear reference value for a national scale where we have various environments and catchment characteristics. A shortcoming of this approach is that it does not fully capture the wide range of event types, from fast, sub-hourly convective rainfall to events lasting more than 10 h, for which antecedent conditions and accumulated moisture play an important role.

Due to its broad application and the relatively high DEM resolution (5 m), LSHIM of debris flows remains an automated hazard indication method. Detailed hazard maps at specific sites are as of now out of scope. Though numerical simulations are often preferred by stakeholders, there are no requirements for parametrization. This raises concerns about the accuracy of these approaches (Graf et al., 2019). Also, despite this research having a large number of validation points and a well-setup calibration around these, still more events and over longer time-ranges could increase confidence in our susceptibility and therefore hazard indication maps (Graf et al., 2019).

Deterministic scenario modeling fails to take feedback mechanisms and parameter inter-variability into account. For example, through time not every precipitation event with a specific return period is associated with a fixed sediment availability (Liu et al., 2025). This is well documented in the analysis of 61 debris flow torrents in Gertsch and Kienholz (2008) or in the margin of stability concept by Steger et al. (2024). This could lead to an overestimation of hazard (Liu et al., 2025). In general, it is important to also take into account the change in sediment budget, which can nullify a possible increased extreme precipitation (Frank et al., 2019). Also debris flow triggering is not guaranteed for comparable rainfall events (Baer et al., 2017; Gertsch and Kienholz, 2008). Despite this and in light of the hazard indication (requiring lower standards than full hazard maps) and the large scale of the project, we think our scenarios provide a realistic indication for standardized scenarios of what planners can expect.

7.3 Future work

Large-scale debris-flow modelling provides a solid basis for inter-comparison of debris-flow hazard indication. Shortcomings, as mentioned in Sect. 7.2, can be addressed by future studies. For instance, return-period-dependent sediment availability can be incorporated. This could benefit from a validation not for all known events but by filtering events for known return periods. Lowering the threshold for $P_{\text{Debris flow}}$ could be applied under a more conservative modelling strategy, where false negatives are to be avoided at all costs. Better data availability on potential sediment entrainment as well as a stronger physical basis for its implementation could improve the quality of debris-flow runout modelling. This may prove better than the current central focus on extreme precipitation and its return periods.

Results as presented are limited to the current climate and landscape. Under climate change, conditions will change considerably. Relevant for debris flows are for instance the increase in extreme precipitation MeteoSwiss and ETH Zurich (2025) and profound change in glacial and permafrost extent in alpine areas (Hirschberg et al., 2021). This could result in increased large-volume events such as Glacial lake outburst floods (Zhang et al., 2024) and events related to permafrost degradation (Frank et al., 2019). In our current approach, glaciers provide a buffer effect, which will decrease with disappearing glaciers. We aim to include this as well as results from permafrost degradation as relevant in bulking debris flows in future research.

The method now has a strong deterministic character. We define clear release areas, parametrization and a restriction to 30-, 100-, and 300-year return period periods. Continuous ensemble modelling in a probabilistic fashion (Kleinn et al., 2025) would better quantify uncertainty both in the susceptibility and runout modelling. Our methodology focuses on entrainment in the debris-flow process where magnitude of the event strongly correlates with channel flow accumulation and sediment availability. In nature, large sediment pulses through landslides or releases of degrading permafrost can cause devastating debris flows (Stoffel and Huggel, 2012). Including this process, arguably in a robust probabilistic manner, would be a great improvement. By incorporation up-to-date weather forecasts near real-time modelling for decision making for the management of traffic routes could be aspired. First attempts to do so for snow avalanches have been made by Glaus et al. (2026).

8 Conclusions

This manuscript presents the first national-scale debris-flow hazard indication modelling combining a comprehen-

sive susceptibility and runout analysis. We define susceptible release areas in streams using a random forest, cross-validated the StorMe database, to an accuracy of 0.814 and ROC-AUC of 0.866. Topographic and precipitation attributes are shown to have the highest predictive power. The debris flow dynamics simulation tool RAMMS::LSHIM-Debrisflow, with a spatially variable potential sediment and friction parametrization, is applied for runout modelling. Large differences can be observed across landscapes, with small fluid debris flows in pre-alpine areas, large granular debris flows in the alpine environment that accumulate a multitude of their mass from entrainment and areas with limited sediment availability that are smaller than could be concluded from topography. In total, we simulate 16 756 debris flows, that results in 54.5, 75.8, and 85.2 km of railway line affected by debris flow hazard for a 30-, 100-, and 300-year return period respectively. Subdivision in hazard intensity classes indicates the highest relative increase is in the highest intensity classes under more extreme return periods. This in turn indicates that debris flows under more extreme events tend to expand in flow height rather than spatial extent. The large-scale, but detailed site-specific maximum debris flow height, give unprecedented capacity to the Swiss Federal Railways to prioritize and plan adaptation measures. Limitations in our hazard assessment lie in the accuracy of the PRA definition and deterministic parametrization of erosion potential. These facts underline that this method is to be applied both on the large scale and as hazard indication.

Appendix A

A1 Topography

Table A1. Glossary of topographic data used in the susceptibility analysis. the base DEM also serves in the RAMMS runout calculations.

	Layer	Description	Resolution
1	Base DEM	swissALTI3D (https://www.swisstopo.admin.ch/en/height-model-swissalti3d, last access: 23 July 2024)	0.5 m
2	Slope	Derived in ArcGIS Pro (3 × 3 window) from the base DEM	1 m
3	Northerness	Cosine of aspect; derived in ArcGIS Pro (3 × 3 window) from the base DEM	1 m
4	Easterness	Sine of aspect; derived in ArcGIS Pro (3 × 3 window) from the base DEM	1 m
5	Flow accumulation	D8 flow accumulation derived in ArcGIS Pro from the base DEM	1 m
6	Curvature	Derived in ArcGIS Pro (3 × 3 window) from the base DEM	10 m

A2 Spatial data

Table A2. Glossary of additional raster and vectordata, beside topographic, used in this project. A description and, when available, a link to the data source is provided. Layer 12 requires an area correction because extreme precipitation depth decreases over larger areas. The correction follows the method of Grebner et al. (1999).

	Layer	Description	Resolution
1	Vegetation height	Vegetation height model (LFI); https://www.lfi.ch/en/maps/vegetation-height-surface-model (last access: 5 March 2025)	1 m
2	Forest presence	Topographic Landscape Model – land cover forest; https://www.swisstopo.admin.ch/en/information-topographic-landscape-model (last access: 30 January 2024)	1 m
3	Permafrost	Permafrost and ground ice map; https://www.slf.ch/de/services-und-produkte/permafrost-und-bodeneiskarte/ (last access: 4 June 2025)	10 m
4	Landscape typology	38 landscape-use types; https://www.are.admin.ch/de/landschaftstypologie-schweiz (last access: 12 March 2025)	10 m
5	Rock cover	Topographic Landscape Model – land cover rock/loose rocks/other; https://www.swisstopo.admin.ch/en/information-topographic-landscape-model (last access: 30 January 2024)	10 m
6	Water storage capacity	Federal Office for Agriculture – six classes of available soil water; https://www.geocat.ch/geonetwork/srv/eng/catalog.search#/metadata/6caf4d0f-52da-433a-809f-92781316ad0e (last access: 12 March 2025)	10 m
7	Lithology	GeoCover geological vector database – attribute LITHOLOGY (rasterized); https://www.swisstopo.admin.ch/de/geologisches-modell-2d-geocover (last access: 30 June 2025)	10 m
8	Hydrogeology	GeoCover geological vector database – attribute HYDROGEO (rasterized); https://www.swisstopo.admin.ch/de/geologisches-modell-2d-geocover (last access: 30 June 2025)	10 m
9	Rock type	GeoCover geological vector database – attribute ROCK (rasterized); https://www.swisstopo.admin.ch/de/geologisches-modell-2d-geocover (last access: 30 June 2025)	10 m
10	Tectonic units	GeoCover geological vector database – attribute TECTONIC (rasterized); https://www.swisstopo.admin.ch/de/geologisches-modell-2d-geocover (last access: 30 June 2025)	10 m
11	Yearly precipitation	Climate normals precipitation 1991–2020 (MeteoSwiss); https://www.meteoswiss.admin.ch/climate/the-climate-of-switzerland/climate-normals.html (last access: 21 March 2025)	1000 m
12	1 and 24 h extreme precipitation	MeteoSwiss extreme precipitation maps (1 h duration). Return periods of 30, 100, and 300 years are used in this study; (Fukutome et al., 2025); https://hydromaps.ch/#en/8/46.830/8.193/bl_hds (last access: 19 February 2025)	1000 m
13	Topographic Landscape Model (TLM)	Swiss Topographic Landscape Model (TLM) vector dataset from swisstopo.	–
14	Altschutt/Jungschutt	Attribute list from Geo7 engineering company applied to the GeoCover geological database	
15	StorMe debris flows	StorMe database – Wasser/Murgang category; features containing "Uebermuerung" in the description (total features: 6351); https://www.bafu.admin.ch/bafu/de/home/themen/naturgefahren/gefahrengrundlagen/schaeden/naturereigniskataster-StorMe.html (last access: 13 March 2025)	–
16	StorMe floods	StorMe database – Wasser/Murgang category; features containing "Ueberschwemmung" or "unspezifiziert" in the description (total features: 19 175); https://www.bafu.admin.ch/bafu/de/home/themen/naturgefahren/gefahrengrundlagen/schaeden/naturereigniskataster-StorMe.html (last access: 13 March 2025)	–
17	SGI glacial extent	Swiss Glacier Inventory (SGI) glacier extent dataset.	–
18	GeoCover fans	Alluvial fan polygons derived from the GeoCover geological vector database.	–

A3 Hydrograph properties

A total of 36 statistical properties from 19 layers are assigned to the hydrograph points. Additionally 5 ratios are added giving a total of 41 properties. Ratios are added to enhance performance of statistical models. An overview is given in Table A3 below. Details on data origin are in Sects. A1 and A2.

Table A3. Summary of spatial data layers and derived ratios used as hydrograph properties. CA = Catchment Area, STR = Streamsection, HY = Hydrograph point, MEAN = Mean value, MIN = Minimum value, MAX = Maximum value, RANGE = Range of values, SD = Standard deviation of values, PV = Point value, MAJ = Majority value. Note that for boolean raster (e.g. Forest presence, Permafrost) the mean value equals the percentage in the catchment area.

	Layer	Category	Statistical properties
1	DEM	Topography	CA: MEAN, MIN, MAX, RANGE, SD; STR: MEAN, MIN, MAX, RANGE, SD
2	Slope	Topography	CA: MEAN; STR: MEAN, SD
3	Northerness	Topography	CA: MEAN, SD
4	Easterness	Topography	CA: MEAN
5	Flow Accumulation	Topography	CA: MEAN, SD; STR: MEAN, SD; HY: PV
6	Curvature	Topography	STR: MEAN, SD
7	Vegetation height	Vegetation	CA: MEAN
8	Forest presence	Vegetation	CA: MEAN
9	Permafrost	Glaciology	CA: MEAN
10	Glacier presence	Glaciology	CA: MEAN
11	Landscape typology	Geomorphology	CA: MAJ
12	Land cover	Geomorphology	CA: MAJ
13	Water storage capacity	Geomorphology	CA: MAJ
14	Lithology	Geology	CA: MAJ
15	Hydrogeology	Geology	CA: MAJ
16	Rock type	Geology	CA: MAJ
17	Tectonic units	Geology	CA: MAJ
18	Extreme rainfall 1 h, $T = 100$ year	Climate	CA: MEAN
19	Extreme rainfall 24 h, $T = 100$ year	Climate	CA: MEAN
20	Yearly precipitation	Climate	CA: MEAN
Additional Ratios with description			
21	Stream linearity	–	Euclidean distance/length of the stream section
22	Catchment roundness	–	CA perimeter/CA area
23	Melton ratio	–	Elevation range/$\sqrt{\text{Flow Accumulation}}$
24	1 h P ratio	–	Extreme rainfall 1 h, $T = 100$ year/yearly precipitation
25	24 h P ratio	–	Extreme rainfall 24 h, $T = 100$ year/yearly precipitation

A4 Erosion parametrization

Table A4. RAMMS erosion parameters by erosion class.

Erosion class	Erosion rate [$\mathrm{m\,s^{-1}}$]	Potential erosion depth per unit basal shear stress [$\mathrm{m\,kPa^{-1}}$]	Critical stress [kPa]
High	0.05	0.20	0.5
Medium (default)	0.025	0.10	1.0
Low	0.0125	0.05	1.5
No erosion	0	0	1.5

Table A5. RAMMS potential erosion depth for different erosion classes and return periods.

Erosion class	Return period [year]	Maximum erosion depth [m]
High	300	4.00
High	100	1.00
High	30	0.33
Medium	300	2.00
Medium	100	0.50
Medium	30	0.17
Low	300	1.00
Low	100	0.25
Low	30	0.08
No erosion	300	0.00
No erosion	100	0.00
No erosion	30	0.00

Appendix B

B1 Dornibach event



Figure B1. Illustrations from the Dornibach railway crossing in Canton Uri, Switzerland. Upper left is before the event. Other illustrations show the railway infrastructure after the event of 24 August 2005. Images supplied by the SBB.

Code and data availability. Hazard indication maps as well as GIS workflow (python in ArcGIS pro) to produce these maps are not available given the commercial character of the project in which it was generated. Examples as used in this manuscript are available upon request. Due to the sensitivity to hazard indication maps we like to state that example maps presented in this research do not give any guarantees. Local hazard should still be validated by experts.

Author contributions. FBvZ and MB conceived the study and developed the methodology. MB integrated our methods with Swiss hazard standards. YB provided expert input and feedback throughout the development of the study. FBvZ performed the data analysis and produced the figures. FBvZ wrote the manuscript with contributions to specific sections from all co-authors. All authors reviewed and approved the final manuscript.

Competing interests. At least one of the (co-)authors is a member of the editorial board of *Natural Hazards and Earth System Sciences*. The peer-review process was guided by an independent editor, and the authors also have no other competing interests to declare.

Disclaimer. Publisher's note: Copernicus Publications remains neutral with regard to jurisdictional claims made in the text, published maps, institutional affiliations, or any other geographical representation in this paper. The authors bear the ultimate responsibility for providing appropriate place names. Views expressed in the text are those of the authors and do not necessarily reflect the views of the publisher.

Acknowledgements. We thank Marc Hauser and Florian Hofstetter from the Swiss Federal Railways for the initiation and the financial support to the Multi-Hazard-Risk Framework Project within the WSL Research Programme CCAMM (http://ccamm.slf.ch, last access: 16 November 2026), to which this project belongs. We appreciated the fruitful discussions over the years and thank them for allowing us to share excerpts from the project results in this manuscript. Catherine Berger, Peter Mani and Michael Rinderer from geo7 provided valuable input and feedback on the methodology during project meetings. Damian Stoffel and Tim Steffen from the Bau- und Verkehrsdirektion des Kantons Bern, Tiefbauamt, Oberingenieurkreis I helped us with interpreting and classifying debris flows in pre-alpine areas. Sophie Fukutome and Jan Raczak from MeteoSchweiz guided us in the available extreme-precipitation data and provided their expert knowledge. Marc Christen from RAMMS AG assisted us in the application of RAMMS and developed the LSHIM version applied in this manuscript. Pia Echtler at SLF assisted us with the random forest application and with her review of the project documentation. Brian McArdell from WSL advised us in the methodology with his broad experience in debris-flow behavior. We thank all persons involved for their support. Finally, we thank two anonymous reviewers whose constructive comments on the preprint of this manuscript helped us to better motivate parametrization choices and substantially improve the quality of the manuscript.

Review statement. This paper was edited by Ugur Öztürk and reviewed by two anonymous referees.

References

Abancó, C. and Hürlimann, M.: Estimate of the debris-flow entrainment using field and topographical data, Nat. Hazards, 71, 363–383, https://doi.org/10.1007/s11069-013-0930-5, 2014.

Baer, P., Huggel, C., McArdell, B. W., and Frank, F.: Changing debris flow activity after sudden sediment input: a case study from the Swiss Alps, Geology Today, 33, 216–223, https://doi.org/10.1111/gto.12211, 2017.

BAFU: Schutz vor Massenbewegungsgefahren. Vollzugshilfe für das Gefahrenmanagement von Rutschungen, Steinschlag und Hangmuren, BAFU, Bern, https://www.bafu.admin.ch/de/vollzugshilfen-naturgefahren (last access: 14 May 2026), 2016.

Baggio, T., Martini, M., Bettella, F., and D'Agostino, V.: Debris flow and debris flood hazard assessment in mountain catchments, CATENA, 245, 108338, https://doi.org/10.1016/j.catena.2024.108338, 2024.

Berger, C., McArdell, B. W., and Schlunegger, F.: Direct measurement of channel erosion by debris flows, Illgraben, Switzerland, J. Geophys. Res.-Earth, 116, F01002, https://doi.org/10.1029/2010JF001722, 2011.

Bernard, M., Barbini, M., Berti, M., Boreggio, M., Simoni, A., and Gregoretti, C.: Rainfall runoff modeling in rocky headwater catchments for the prediction of debris flow occurrence, Water Resour. Res., 61, e2023WR036887, https://doi.org/10.1029/2023WR036887, 2025.

Beven, K. J.: A history of the concept of time of concentration, Hydrol. Earth Syst. Sci., 24, 2655–2670, https://doi.org/10.5194/hess-24-2655-2020, 2020.

Bolliger, D., Schlunegger, F., and McArdell, B. W.: Comparison of debris flow observations, including fine-sediment grain size and composition and runout model results, at Illgraben, Swiss Alps, Nat. Hazards Earth Syst. Sci., 24, 1035–1049, https://doi.org/10.5194/nhess-24-1035-2024, 2024.

Bonomelli, R., Pilotti, M., and Farina, G.: Use of simple analytical solutions in the calibration of shallow water equation debris flow models, Earth Surf. Dynam., 13, 665–681, https://doi.org/10.5194/esurf-13-665-2025, 2025.

Breiman, L.: Random forests, Mach. Learn., 45, 5–32, 2001.

Bründl, M., Romang, H. E., Bischof, N., and Rheinberger, C. M.: The risk concept and its application in natural hazard risk management in Switzerland, Nat. Hazards Earth Syst. Sci., 9, 801–813, https://doi.org/10.5194/nhess-9-801-2009, 2009.

Bründl, M., Ortner, G., Bühler, Y., Bebi, P., M., C., Kissling, E., Michel, A., Spieler, M., Völk, M., and Zaugg, A.: Task 3.1–Multi-hazard risk assessment framework, in: WSL Research Program Climate Change Impacts on Alpine Mass Movements – CCAMM Project Report, Eidg. Forschungsanstalt WSL, https://doi.org/10.55419/wsl:41905, 2025.

Bühler, Y., Bebi, P., Christen, M., Margreth, S., Stoffel, L., Stoffel, A., Marty, C., Schmucki, G., Caviezel, A., Kühne, R., Wohlwend, S., and Bartelt, P.: Automated avalanche hazard indication mapping on a statewide scale, Nat. Hazards Earth Syst. Sci., 22, 1825–1843, https://doi.org/10.5194/nhess-22-1825-2022, 2022.

Bühlmann, A. and Schwanbeck, J.: Bilanzierungsgebiete, in: Daten- und Analyseplattform, Hydrologischer Atlas der Schweiz, https://hydromaps.ch/#de/8/46.830/8.190/bl_hds--a02_a02_palps_yr_02_bilanz_clean_topo$0/NULL (last access: 28 April 2025), 2018.

Bundesamt für Forstwesen (BFF) and Eidg. Institut für Schnee- und Lawinenforschung (SLF): Richtlinien zur Berücksichtigung der Lawinengefahr bei raumwirksamen Tätigkeiten, EDMZ, Bern, https://www.bafu.admin.ch/dam/de/sd-web/bloPDp22w9ZQ/richtlinien-lawinengefahr-raumwirksame-taetigkeiten-1984.pdf (last access 2 May 2026), 1984.

Cannon, S. H., Gartner, J. E., Parrett, C., and Parise, M.: Wildfire-related debris-flow generation through episodic progressive sediment-bulking processes, western USA, in: Debris-Flow Hazards Mitigation: Mechanics, Prediction, and Assessment, Millpress, Rotterdam, 71–82, ISBN 978-90-77017-78-4, 2003.

Cavagnaro, D. B., McCoy, S. W., Kean, J. W., Thomas, M. A., Lindsay, D. N., McArdell, B. W., and Hirschberg, J.: A robust quantitative method to distinguish runoff generated debris flows from floods, Geophys. Res. Lett., 51, e2024GL109768, https://doi.org/10.1029/2024GL109768, 2024.

Cavagnaro, D. B., McCoy, S. W., Lindsay, D. N., McGuire, L. A., Kean, J. W., and Trugman, D. T.: Rainfall thresholds for postfire debris flow initiation vary with short duration rainfall climatology, J. Geophys. Res.-Earth, 130, https://doi.org/10.1029/2024jf007781, 2025.

Chen, T. and Guestrin, C.: XGBoost: A Scalable Tree Boosting System, in: Proceedings of the 22nd ACM SIGKDD International Conference on Knowledge Discovery and Data Mining, 785–794, https://doi.org/10.1145/2939672.2939785, 2016.

Chiarle, M., Iannotti, S., Mortara, G., and Deline, P.: Recent debris flow occurrences associated with glaciers in the Alps, Global Planet. Change, 56, 123–136, https://doi.org/10.1016/j.gloplacha.2006.07.003, 2007.

Christen, M., Kowalski, J., and Bartelt, P.: RAMMS: numerical simulation of dense snow avalanches in three-dimensional terrain, Cold Reg. Sci. Technol., 63, 1–14, https://doi.org/10.1016/j.coldregions.2010.04.005, 2010.

Church, M. and Jakob, M.: What is a debris flood?, Water Resour. Res., 56, e2020WR027144, https://doi.org/10.1029/2020WR027144, 2020.

Crescenzo, L., Guthrie, R., and Calvello, M.: Evaluating the performance of propagation models of flow-like landslides at regional scale, Landslides, 21, 229–243, https://doi.org/10.1007/s10346-023-02162-z, 2024.

Davies, T. R.: Large and small debris flows – Occurrence and behaviour, in: Recent Developments on Debris Flows, edited by: Armanini, A. and Michiue, M., Vol. 64, Springer Berlin Heidelberg, Berlin, Heidelberg, series Title: Lecture Notes in Earth Sciences, https://doi.org/10.1007/BFb0117760, 27–45, 1997.

Davies, T., Bloomberg, M., Palmer, D., and Robinson, T.: Debris-flow risk-to-life: preliminary screening, Int. J. Disast. Risk. Re., 100, 104158, https://doi.org/10.1016/j.ijdrr.2023.104158, 2024.

Delmonaco, G., Leoni, G., Margottini, C., Puglisi, C., and Spizzichino, D.: Large scale debris-flow hazard assessment: a geotechnical approach and GIS modelling, Nat. Hazards Earth Syst. Sci., 3, 443–455, https://doi.org/10.5194/nhess-3-443-2003, 2003.

Dixit, S., Siva Subramanian, S., Srivastava, P., Yunus, A. P., Martha, T. R., and Sen, S.: Numerical-model-derived intensity–duration thresholds for early warning of rainfall-induced debris flows in a Himalayan catchment, Nat. Hazards Earth Syst. Sci., 24, 465–480, https://doi.org/10.5194/nhess-24-465-2024, 2024.

Drucker, H., Burges, C. J. C., Kaufman, L., Smola, A., and Vapnik, V.: Support vector regression machines, in: Advances in Neural Information Processing Systems, Vol. 9, MIT Press, 155–161, https://proceedings.neurips.cc/paper/1996/hash/d38901788c533e8286cb6400b40b386d-Abstract.html (last access: 10 August 2026), 1996.

Esri: ArcGIS Pro, Computer software, Version 3.3, https://www.esri.com/arcgis (last access: 28 January 2025), 2024.

Eu, S. and Im, S.: The effect of entrainment model on debris-flow simulation – comparison of two simple 1D models, Water-Sui., 17, 761, https://doi.org/10.3390/w17050761, 2025.

Fan, L., Lehmann, P., McArdell, B., and Or, D.: Linking rainfall-induced landslides with debris flows runout patterns towards catchment scale hazard assessment, Geomorphology, 280, 1–15, https://doi.org/10.1016/j.geomorph.2016.10.007, 2017.

Federal Office for the Environment FOEN: State of Natural Hazards, https://www.bafu.admin.ch/en/state-naturalhazards (last access: 7 July 2026), 2025.

Federal Office of Topography swisstopo: Geologischen Vektordaten (GeoCover) V3 1 : 25 000, https://www.swisstopo.admin.ch/de/geologisches-modell-2d-geocover(last access: 30 June 2025), 2024a.

Federal Office of Topography swisstopo: The Topographic Landscape Model TLM – Ground cover, https://www.swisstopo.admin.ch/en/information-topographic-landscape-model (last access: 30 January 2024), 2024b.

Federal Office of Topography swisstopo: swissALTI3D, digital elevation model (DEM), 0.5 m resolution; https://www.swisstopo.admin.ch/en/height-model-swissalti3d (last access: 4 June 2026), 2024c.

Fischer, E., Wolken, G. J., Bühler, Y., Christen, M., and Lader, R.: Automated Avalanche Hazard Indication for Southeast Alaska, EGUsphere [preprint], https://doi.org/10.5194/egusphere-2026-1345, 2026.

Frank, F., McArdell, B. W., Huggel, C., and Vieli, A.: The importance of entrainment and bulking on debris flow runout modeling: examples from the Swiss Alps, Nat. Hazards Earth Syst. Sci., 15, 2569–2583, https://doi.org/10.5194/nhess-15-2569-2015, 2015.

Frank, F., McArdell, B. W., Oggier, N., Baer, P., Christen, M., and Vieli, A.: Debris-flow modeling at Meretschibach and Bondasca catchments, Switzerland: sensitivity testing of field-data-based entrainment model, Nat. Hazards Earth Syst. Sci., 17, 801–815, https://doi.org/10.5194/nhess-17-801-2017, 2017.

Frank, F., Huggel, C., McArdell, B. W., and Vieli, A.: Landslides and increased debris flow activity: a systematic comparison of six catchments in Switzerland, Earth Surf. Proc. Land., 44, 699–712, https://doi.org/10.1002/esp.4524, 2019.

Fukutome, S., Alouini, S., and Frei, C.: Extreme Point Precipitation (B04), hydromaps product B04, https://hydrologischeratlas.ch (last access: 19 February 2025), 2023.

Fukutome, S., Alouini, S., and Frei, C.: Extreme Punktniederschläge, in: Daten- und Analyseplattform, Hydrologischer Atlas der Schweiz, https://hydromaps.ch/#de/8/46.832/8.190/bl_

hds--b04_b0401_precip_60m_2a_0_5v2_0$4/NULL (last access: 19 February 2025), 2025.

Gertsch, E. and Kienholz, H.: Geschiebelieferung alpiner Wildbachsysteme bei Großereignissen, in: INTERPRAEVENT 2008 Conference Proceedings, Vol. 1, Internationale Forschungsgesellschaft INTERPRAEVENT, Klagenfurt, Austria, 331–342, ISBN 978-3-901164-10-1, 2008.

Glaus, J., Kleinn, J., Stoffel, L., Ruttner, P., Wikstrom Jones, K., Gaume, J., and Bühler, Y.: Probability indication maps for avalanche runout for decision support in daily traffic rout risk management, The Cryosphere, 20, 6087–6106, https://doi.org/10.5194/tc-20-6087-2026, 2026.

Goodfellow, I., Bengio, Y., and Courville, A.: Deep Learning, MIT Press, ISBN 978-0-262-03561-3, 2016.

Graf, C., Christen, M., McArdell, B. W., and Bartelt, P.: Overview of a decade of applied debris-flow runout modeling in Switzerland: Challenges and recommendations, in: Debris-Flow Hazards Mitigation: Mechanics, Monitoring, Modeling, and Assessment, edited by: Kean, J. W., Coe, J. A., Santi, P. M., and Guillen, B. K., Association of Environmental and Engineering Geologists, Golden, Colorado, USA, 685–692, https://doi.org/10.25676/11124/173155, 2019.

Grebner, D., Roesch, T., and Schwarb, M.: Extreme Gebietsniederschläge unterschiedlicher Dauer und Wiederkehrperioden 1981–1993, in: Hydrologischer Atlas der Schweiz, Bundesamt für Wasser und Geologie, Bern, https://www.dora.lib4ri.ch/wsl/dload/wsl:20639/PDF/Bundesamt_f%C3%BCr_Wasser_und_Geologie_BWG-2000-Hochwasser_1999._Analyse_der_Ereignisse-(published_version).pdf (last access: 15 May 2025), 1999.

Harris, J. K.: Primer on binary logistic regression, BMJ Family Medicine and Community Health, 9, e001290, https://doi.org/10.1136/fmch-2021-001290, 2021.

Hauser, D.: Interaktion Murgang–Wald: Rekonstruktion von Ereignissen mit Hilfe von RAMMS, Master's thesis, ETH Zürich, Zürich, Switzerland, https://doi.org/10.3929/ethz-a-006455792, 2011.

Hirschberg, J., McArdell, B. W., Badoux, A., and Molnar, P.: Analysis of rainfall and runoff for debris flows at the Illgraben catchment, Switzerland, Geophysical Research Abstracts, 21, 693–700, 2019.

Hirschberg, J., Fatichi, S., Bennett, G. L., McArdell, B. W., Peleg, N., Lane, S. N., and Molnar, P.: Climate change impacts on sediment yield and debris-flow activity in an alpine catchment, J. Geophys. Res.-Earth, 126, e2020JF005739, https://doi.org/10.1029/2020JF005739, 2021.

Horton, P., Jaboyedoff, M., Rudaz, B., and Zimmermann, M.: Flow-R, a model for susceptibility mapping of debris flows and other gravitational hazards at a regional scale, Nat. Hazards Earth Syst. Sci., 13, 869–885, https://doi.org/10.5194/nhess-13-869-2013, 2013.

Hürlimann, M., Rickenmann, D., and Graf, C.: Field and monitoring data of debris-flow events in the Swiss Alps, Can. Geotech. J., 40, 161–175, https://doi.org/10.1139/t02-087, 2003.

Hürlimann, M., Copons, R., and Altimir, J.: Detailed debris flow hazard assessment in Andorra: a multidisciplinary approach, Geomorphology, 78, 359–372, https://doi.org/10.1016/j.geomorph.2006.02.003, 2006.

Hürlimann, M., McArdell, B. W., and Rickli, C.: Field and laboratory analysis of the runout characteristics of hillslope debris flows in Switzerland, Geomorphology, 232, 20–32, https://doi.org/10.1016/j.geomorph.2014.11.030, 2015.

Iadanza, C., Trigila, A., and Napolitano, F.: Identification and characterization of rainfall events responsible for triggering of debris flows and shallow landslides, J. Hydrol., 541, 230–245, 2016.

Issler, D., Gisnås, K. G., Gauer, P., Glimsdal, S., Domaas, U., and Sverdrup-Thygeson, K.: Naksin – a new approach to snow avalanche hazard indication mapping in Norway, SSRN, https://doi.org/10.2139/ssrn.4530311, 2023.

Iverson, R. M.: Debris flows: behaviour and hazard assessment, Geology Today, 30, 15–20, https://doi.org/10.1111/gto.12037, 2014.

Jansson, P., Hock, R., and Schneider, T.: The concept of glacier storage: a review, J. Hydrol., 282, 116–129, https://doi.org/10.1016/S0022-1694(03)00258-0, 2003.

Keck, J., Istanbulluoglu, E., Campforts, B., Tucker, G., and Horner-Devine, A.: A landslide runout model for sediment transport, landscape evolution, and hazard assessment applications, Earth Surf. Dynam., 12, 1165–1191, https://doi.org/10.5194/esurf-12-1165-2024, 2024.

Kenner, R., Noetzli, J., Hoelzle, M., Raetzo, H., and Phillips, M.: Distinguishing ice-rich and ice-poor permafrost to map ground temperatures and ground ice occurrence in the Swiss Alps, The Cryosphere, 13, 1925–1941, https://doi.org/10.5194/tc-13-1925-2019, 2019.

Kienholz, H., Frick, E., and Gertsch, E.: Assessment tools for mountain torrents: SEDEX© and bed load assessment matrix, in: Proceedings of the International Symposium INTERPRAEVENT 2010 in the Pacific Rim, Taipei, Taiwan, 245–256, https://www.tur.ch/wp-content/uploads/turPublikation_Kienholz-et-al_2010_SEDEXAssessmentMatrix.pdf (last access: 3 April 2026), 2010.

Kim, H.-S., Chung, C.-K., Kim, S.-R., and Kim, K.-S.: A GIS-based framework for real-time debris-flow hazard assessment for expressways in Korea, Int. J. Disast. Risk. Sc., 7, 293–311, https://doi.org/10.1007/s13753-016-0096-3, 2016.

Kleinn, J., Bühler, Y., Glaus, J., Aller, D., Berger, C., Rinderer, M., Hählen, N., Peter, A., and Singeisen, C.: A probability-based modelling approach beyond a few selected return periods for comprehensive and robust hazard and risk assessment, in: Proceedings of the International Snow Science Workshop, Tromsø, Norway, 23–29 September 2024, 841–847, https://arc.lib.montana.edu/snow-science/objects/ISSW2024_O7.7.pdf (last access: 11 September 2026), 2024.

Kleinn, J., Berger, C., Aller, D., Rinderer, M., Hählen, N., Peter, A., Singeisen, C., and Jordi, M.: Pro-Mo: probabilistische Gefahren- und Risikomodellierung für gravitative Naturgefahren. Schlussbericht zum Pilotprojekt, WSL-Berichte: Vol. 177, Birmensdorf, https://doi.org/10.55419/wsl:41550, 2025.

Klok, E. J., Jasper, K., Roelofsma, K. P., Gurtz, J., and Badoux, A.: Distributed hydrological modelling of a heavily glaciated Alpine river basin, Hydrolog. Sci. J., 46, 553–570, https://doi.org/10.1080/02626660109492850, 2001.

Klubertanz, G., Laloui, L., and Vulliet, L.: Identification of mechanisms for landslide type initiation of debris flows, Eng. Geol.,

109, 114–123, https://doi.org/10.1016/j.enggeo.2009.06.007, 2009.

Kritikos, T. and Davies, T.: Assessment of rainfall-generated shallow landslide/debris-flow susceptibility and runout using a GIS-based approach: application to western Southern Alps of New Zealand, Landslides, 12, 1051–1075, https://doi.org/10.1007/s10346-014-0533-6, 2015.

Kumar, S., Sharma, A., and Singh, K.: A comprehensive review on debris flow landslide assessment using rapid mass movement simulation (RAMMS), Geotechnical and Geological Engineering, 42, 5447–5475, https://doi.org/10.1007/s10706-024-02887-1, 2024.

Lee, S., An, H., Kim, M., and Kang, T.: Numerical analysis of dynamics between debris flows and wave propagation using multi-layer shallow water equations, EGUsphere [preprint], https://doi.org/10.5194/egusphere-2025-1383, 2025.

Linsbauer, A., Huss, M., Hodel, E., Bauder, A., Fischer, M., Weidmann, Y., Bärtschi, H., and Schmassmann, E.: The new Swiss Glacier inventory SGI2016: from a topographical to a glaciological dataset, Front. Earth Sci., 9, 704189, https://doi.org/10.3389/feart.2021.704189, 2021.

Liu, J., He, P., Xiao, J., Hu, Q., Ren, Y., Kornejady, A., and Gao, H.: When time prevails: the perils of overlooking temporal landscape evolution in landslide susceptibility predictions, Remote Sens.-Basel, 17, 1752, https://doi.org/10.3390/rs17101752, 2025.

Loat, R. and Petrascheck, A.: Berücksichtigung der Hochwassergefahren bei raumwirksamen Tätigkeiten. Empfehlungen, BWW, BRP, BUWAL, https://www.bafu.admin.ch/dam/de/sd-web/nuOUwFjyeUSV/ (last access: 24 April 2026), 1997.

Marchi, L., Brunetti, M. T., Cavalli, M., and Crema, S.: Debris flow volumes in northeastern Italy: relationship with drainage area and size probability, Earth Surf. Proc. Land., 44, 933–943, https://doi.org/10.1002/esp.4546, 2019.

McGuire, L. A., McCoy, S. W., Marc, O., Struble, W., and Barnhart, K. R.: Steady-state forms of channel profiles shaped by debris flow and fluvial processes, Earth Surf. Dynam., 11, 1117–1143, https://doi.org/10.5194/esurf-11-1117-2023, 2023.

McGuire, L. A., Rengers, F. K., Youberg, A. M., Gorr, A. N., Hoch, O. J., Beers, R., and Porter, R.: Characteristics of debris-flow-prone watersheds and debris-flow-triggering rainstorms following the Tadpole Fire, New Mexico, USA, Nat. Hazards Earth Syst. Sci., 24, 1357–1379, https://doi.org/10.5194/nhess-24-1357-2024, 2024.

Melelli, L. and Taramelli, A.: An example of debris-flows hazard modeling using GIS, Nat. Hazards Earth Syst. Sci., 4, 347–358, https://doi.org/10.5194/nhess-4-347-2004, 2004.

MeteoSwiss: The Climate of Switzerland, https://www.meteoswiss.admin.ch/climate/the-climate-of-switzerland.html, last access: 7 July 2026.

MeteoSwiss and ETH Zurich: Climate CH2025 – Scientific Report, Tech. rep., Federal Office of Meteorology and Climatology MeteoSwiss, Zurich, Switzerland, https://doi.org/10.18751/climate/scenarios/ch2025/sr/1.0, 2025.

Miller, D. J. and Burnett, K. M.: A probabilistic model of debris-flow delivery to stream channels, demonstrated for the Coast Range of Oregon, USA, Geomorphology, 94, 184–205, https://doi.org/10.1016/j.geomorph.2007.05.009, 2008.

Morel, M., Piton, G., Kuss, D., Evin, G., and Le Bouteiller, C.: Statistical modeling of sediment supply in torrent catchments of the northern French Alps, Nat. Hazards Earth Syst. Sci., 23, 1769–1787, https://doi.org/10.5194/nhess-23-1769-2023, 2023.

Napoli, M. D., Tanyas, H., Castro-Camilo, D., Calcaterra, D., Cevasco, A., Martire, D. D., Pepe, G., Brandolini, P., and Lombardo, L.: On the estimation of landslide intensity, hazard and density via data-driven models, https://doi.org/10.21203/rs.3.rs-2984450/v1, 2023.

Naqvi, M. W., Kc, D., and Hu, L.: A case study of the debris flows event in the Chalk Cliffs Basin, Colorado, USA: numerical simulations based on a multi-phase flow model, Water-Sui., 17, 406, https://doi.org/10.3390/w17030406, 2025.

Ortner, G., Bründl, M., Kropf, C. M., Röösli, T., Bühler, Y., and Bresch, D. N.: Large-scale risk assessment on snow avalanche hazard in alpine regions, Nat. Hazards Earth Syst. Sci., 23, 2089–2110, https://doi.org/10.5194/nhess-23-2089-2023, 2023.

Ortner, G., Michel, A., Kropf, C. M., Bründl, M., and Bresch, D. N.: Assessing the impacts of climate change on snow avalanche-induced risk in alpine regions, Nat. Hazards, https://doi.org/10.1007/s11069-025-07229-9, 2025a.

Ortner, G., Michel, A., Spieler, M. B. A., Christen, M., Bühler, Y., Bründl, M., and Bresch, D. N.: A novel approach for bridging the gap between climate change scenarios and avalanche hazard indication mapping, Cold Reg. Sci. Technol., 230, 104355, https://doi.org/10.1016/j.coldregions.2024.104355, 2025b.

Pedregosa, F., Varoquaux, G., Gramfort, A., Michel, V., Thirion, B., Grisel, O., Blondel, M., Prettenhofer, P., Weiss, R., Dubourg, V., and others: Scikit-learn: machine learning in Python, J. Mach. Learn. Res., 12, 2825–2830, 2011.

Prokhorenkova, L., Gusev, G., Vorobev, A., Dorogush, A. V., and Gulin, A.: CatBoost: unbiased boosting with categorical features, arXiv [preprint], https://doi.org/10.48550/arXiv.1706.09516 2018.

Qie, J., Corona, C., Favillier, A., Gubler, S., Estermann, T., and Stoffel, M.: Hydrometeorological triggers of debris flows derived from historical archives and tree-ring data: insights from the Swiss National Park, Sci. Total Environ., 968, 178880, https://doi.org/10.1016/j.scitotenv.2025.178880, 2025.

RAMMS AG: RAMMS::Debrisflow User Manual, version 1.8.0, https://ramms.ch/manuals/RAMMS_DBF_Manual.pdf (last access: 23 June 2026), 2024.

Rickenmann, D.: Empirical relationships for debris flows, Nat. Hazards, 19, 47–77, https://doi.org/10.1023/A:1008064220727, 1999.

Rickenmann, D. and Scheidl, C.: Modelle zur Abschätzung des Ablagerungsverhaltens von Murgängen, Wasser Energie Luft, 102, 17–26, 2010.

Rickenmann, D. and Scheidl, C.: Modelling of debris-flow deposition: terrain slope, mobility coefficient, and back-calculated basal friction coefficient, E3S Web Conf., 415, 07013, https://doi.org/10.1051/e3sconf/202341507013, 2023.

Rickenmann, D. and Zimmermann, M.: The 1987 debris flows in Switzerland: documentation and analysis, Geomorphology, 8, 175–189, https://doi.org/10.1016/0169-555X(93)90036-2, 1993.

Rickenmann, D., Koschni, A., Chiari, M., Scheidl, C., and Canuto, N.: Abschätzung von Feststofffrachten in Wildbächen und Gebirgsflüssen, in: Ereignisanalyse Hochwasser 2005, Teil 2: Analyse von Prozessen, Massnahmen und Gefahrengrundlagen, edited by: Bezzola, G. R. and Hegg, C., Umwelt-Wissen Nr. 0825 (UW-0825-D), Bundesamt für Umwelt (BAFU) and

Eidgenössische Forschungsanstalt WSL, Birmensdorf, 152–162, 2008.

Roelofs, L., Nota, E. W., Flipsen, T. C. W., Colucci, P., and De Haas, T.: How bed composition affects erosion by debris flows – an experimental assessment, Geophys. Res. Lett., 50, e2023GL103294, https://doi.org/10.1029/2023GL103294, 2023.

Salm, B.: Flow, flow transition and runout distances of flowing avalanches, Ann. Glaciol., 18, 221–226, https://doi.org/10.3189/S0260305500011551, 1993.

Savina, M., Brunner, P., Pavic, M., and Rossi, M.: A Short History of Natural Catastrophes in Switzerland, Tech. rep., SCOR, Zurich, Switzerland, https://www.scor.com/sites/default/files/2020_05_-_scor_memo_nat_cat_in_switzerland_final.pdf (last access: 23 April 2026), 2020.

Scheidl, C. and Rickenmann, D.: TopFlowDF – a simple gis based model to simulate debris-flow runout on the fan, Italian Journal of Engineering Geology and Environment, 253–262, https://doi.org/10.4408/IJEGE.2011-03.B-030, 2011.

Scheidl, C., Rickenmann, D., and McArdell, B. W.: Runout prediction of debris flows and similar mass movements, in: Landslide Science and Practice, edited by: Margottini, C., Canuti, P., and Sassa, K., Springer Berlin Heidelberg, Berlin, Heidelberg, https://doi.org/10.1007/978-3-642-31310-3_30, 221–229, 2013.

Schöffl, T., Nagl, G., Koschuch, R., Schreiber, H., Hübl, J., and Kaitna, R.: A perspective of surge dynamics in natural debris flows through pulse Doppler radar observations, J. Geophys. Res.-Earth, 128, e2023JF007171, https://doi.org/10.1029/2023JF007171, 2023.

Shah, N. A., Shafique, M., Owen, L. A., AI-Mulla, Y., and Ullah, Y.: Morphometric analysis of debris flow hazard and risk assessment in the mountain terrains of northern Pakistan using remote sensing and field data, Earth Sci. Inform., 18, 295, https://doi.org/10.1007/s12145-025-01807-y, 2025.

Shen, P., Zhang, L., Chen, H., and Gao, L.: Role of vegetation restoration in mitigating hillslope erosion and debris flows, Eng. Geol., 216, 122–133, https://doi.org/10.1016/j.enggeo.2016.11.019, 2017.

Shen, P., Zhang, L., Wong, H. F., Peng, D., Zhou, S., Zhang, S., and Chen, C.: Debris flow enlargement from entrainment: a case study for comparison of three entrainment models, Eng. Geol., 270, 105581, https://doi.org/10.1016/j.enggeo.2020.105581, 2020.

SIA: SIA norm 261/1:2020 Bauwesen 505 261/1, https://shop.sia.ch/normenwerk/ingenieur/261-1_2020_d/D/Product (last access: 9 November 2026), 2020.

Simoni, A., Bernard, M., Berti, M., Boreggio, M., Lanzoni, S., Stancanelli, L. M., and Gregoretti, C.: Runoff generated debris flows: observation of initiation conditions and erosion–deposition dynamics along the channel at Cancia (eastern Italian Alps), Earth Surf. Proc. Land., 45, 3556–3571, https://doi.org/10.1002/esp.4981, 2020.

Steger, S., Moreno, M., Crespi, A., Luigi Gariano, S., Teresa Brunetti, M., Melillo, M., Peruccacci, S., Marra, F., De Vugt, L., Zieher, T., Rutzinger, M., Mair, V., and Pittore, M.: Adopting the margin of stability for space–time landslide prediction – a data-driven approach for generating spatial dynamic thresholds, Geoscience Frontiers, 15, 101822, https://doi.org/10.1016/j.gsf.2024.101822, 2024.

Stoffel, M. and Huggel, C.: Effects of climate change on mass movements in mountain environments, Progress in Physical Geography: Earth and Environment, 36, 421–439, https://doi.org/10.1177/0309133312441010, 2012.

Stoffel, M., Lièvre, I., Conus, D., Grichting, M. A., Raetzo, H., Gärtner, H. W., and Monbaron, M.: 400 years of debris-flow activity and triggering weather conditions: Ritigraben, Valais, Switzerland, Arct. Antarct. Alp. Res., 37, 387–395, https://doi.org/10.1657/1523-0430(2005)037[0387:yodaat]2.0.co;2, 2005.

Stolz, A. and Huggel, C.: Debris flows in the Swiss National Park: the influence of different flow models and varying DEM grid size on modeling results, Landslides, 5, 311–319, https://doi.org/10.1007/s10346-008-0125-4, 2008.

Struble, W. T., McGuire, L. A., McCoy, S. W., Barnhart, K. R., and Marc, O.: Debris flow process controls on steepland morphology in the San Gabriel Mountains, California, J. Geophys. Res.-Earth, 128, e2022JF007017, https://doi.org/10.1029/2022JF007017, 2023.

Swiss Federal Railways (SBB): SBB Facts and Figures, https://reporting.sbb.ch/ (last access: 4 September 2026), 2026.

Sykes, J., Haegeli, P., and Bühler, Y.: Automated snow avalanche release area delineation in data-sparse, remote, and forested regions, Nat. Hazards Earth Syst. Sci., 22, 3247–3270, https://doi.org/10.5194/nhess-22-3247-2022, 2022.

U.S. Geological Survey: Grfin Tools – User Guide and Methods for Modeling Landslide Runout and Debris-Flow Growth and Inundation, U.S. Geological Survey, Series: Techniques and Methods, https://doi.org/10.3133/tm14A3, 2025.

van Zadelhoff, F. B., Albaba, A., Cohen, D., Phillips, C., Schaefli, B., Dorren, L., and Schwarz, M.: Introducing SlideforMAP: a probabilistic finite slope approach for modelling shallow-landslide probability in forested situations, Nat. Hazards Earth Syst. Sci., 22, 2611–2635, https://doi.org/10.5194/nhess-22-2611-2022, 2022.

Yamanoi, K., Oishi, S., and Kawaike, K.: Prediction of spatial distribution of debris flow hit probability considering the source location uncertainty, J. Flood Risk Manag., 18, https://doi.org/10.1111/jfr3.70011, 2025.

Yang, H., Huang, J., Liu, X., Xu, P., Yu, B., Guo, J., Li, J., Zhou, Y., and Shu, X.: Integration of Morris and GLUE methods for improving massflow-based debris flow simulation, Nat. Hazards, 121, 12589–12612, https://doi.org/10.1007/s11069-025-07289-x, 2025.

Yu, G.-A., Yao, W., Huang, H. Q., and Liu, Z.: Debris flows originating in the mountain cryosphere under a changing climate: a review, Progress in Physical Geography: Earth and Environment, 45, 339–374, https://doi.org/10.1177/0309133320961705, 2021.

Zhang, G., Carrivick, J. L., Emmer, A., Shugar, D. H., Veh, G., Wang, X., Labedz, C. R., Mergili, M., Mölg, N., Huss, M., Allen, S., Sugiyama, S., and Lützow, N.: Characteristics and changes of glacial lakes and outburst floods, Nature Reviews Earth and Environment, 5, 447–462, https://doi.org/10.1038/s43017-024-00554-w, 2024.

Zhang, H.: The optimality of naive bayes, in: Proceedings of the Seventeenth International Florida Artificial Intelligence Research Society Conference (FLAIRS), in: 17th International Florida Artificial Intelligence Research Society Con-

ference (FLAIRS-04), 562–567, https://cdn.aaai.org/FLAIRS/2004/Flairs04-097.pdf (last access: 18 June 2025), 2004.

Zhang, T., Yin, Y., Li, B., Gao, Y., and Wang, M.: Characteristics of two complex rock and glacier avalanches and RAMMS simulation of a long-runout disaster in the Sedongpu Basin of the Yarlung Zangbo River downstream in October 2018, Tibet, China, https://doi.org/10.21203/rs.3.rs-1238705/v1, 2022.

Zimmermann, F., McArdell, B. W., Rickli, C., and Scheidl, C.: 2D runout modelling of hillslope debris flows, based on well-documented events in Switzerland, Geosciences, 10, 70, https://doi.org/10.3390/geosciences10020070, 2020.

Zimmermann, M.: Managing debris flow risks: security measures for a hazard-prone resort in Switzerland, Mt. Res. Dev., 24, 19–23, https://doi.org/10.1659/0276-4741(2004)024[0019:MDFR]2.0.CO;2, 2004.